Inorganic Chemistry

pubs.acs.org/IC Article

Di(hydroperoxy)cycloalkane Adducts of Triarylphosphine Oxides: A Comprehensive Study Including Solid-State Structures and Association in Solution

Fabian F. Arp, Nattamai Bhuvanesh, and Janet Blümel*

Cite This: *Inorg. Chem.* 2020, 59, 13719−13732 Read Online

ACCESS | Metrics & More | Article Recommendations | Supporting Information

ABSTRACT: Four new di(hydroperoxy)cycloalkane adducts (Ahn adducts) of *p*-Tol_3PO (**1**) and *o*-Tol_3PO (**2**), namely, *p*-$Tol_3PO{\cdot}(HOO)_2C(CH_2)_5$ (**3**), *o*-$Tol_3PO{\cdot}(HOO)_2C(CH_2)_5$ (**4**), *p*-$Tol_3PO{\cdot}(HOO)_2C(CH_2)_6$ (**5**), and *o*-$Tol_3PO{\cdot}(HOO)_2C(CH_2)_6$ (**6**), have been synthesized and fully characterized. Their single crystal X-ray structures have been determined and analyzed. The ^{31}P NMR data are in accordance with hydrogen bonding of the di(hydroperoxy)alkanes to the P═O groups of the phosphine oxides. Due to their high solubility in organic solvents, natural abundance ^{17}O NMR spectra of **1**−**6** could be recorded, providing the signals for the P═O groups and additionally the two different oxygen nuclei in the O−OH groups in the adducts **3**−**6**. The association and mobility of **3**−**6** were explored by ^{1}H DOSY (diffusion ordered spectroscopy) NMR, which indicated persistent hydrogen bonding of the adducts in solution. Competition experiments with phosphine oxides allowed ranking of the affinities of the di(hydroperoxy)-cycloalkanes for the different phosphine oxide carriers. On the basis of variable temperature ^{31}P NMR investigations, the Gibbs energies of activation $\Delta G^{\ddagger}$ for the adduct dissociation processes of **3**−**6** at different temperatures, as well as the enthalpy $\Delta H^{\ddagger}$ and entropy $\Delta S^{\ddagger}$ of activation, have been determined. IR spectroscopy of **3**−**6** corroborated the hydrogen bonding, and in the Raman spectra, the ν(O−O) stretching bands have been identified, confirming the presence of peroxy groups in the solid materials. The high solubilities in selected organic solvents have been quantified.

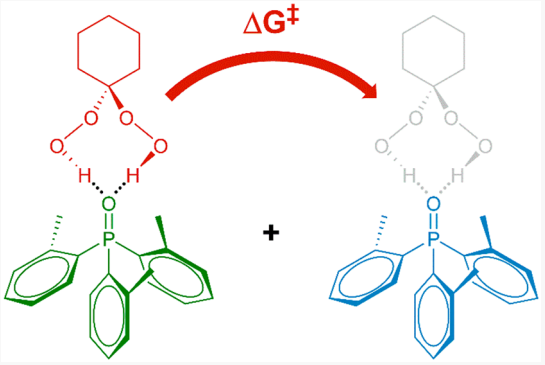

1. INTRODUCTION

1.1. General Introduction. Peroxides are ubiquitous in daily life.[1−3] They are active ingredients for bleaching in the production of goods and for disinfection in the household, in medicine,[4] and wastewater treatment.[5] Peroxides are also employed as radical initiators for polymerizations.[2,6] For synthetic chemistry, oxidation reactions are crucial, and inorganic and organic peroxides, either solo or in the presence of catalysts, play central roles.[1−3] Applications include the oxidation of amines to amides,[7,8] alkane activation,[9,10] epoxidation reactions,[11,12] selective transformations of sulfides to sulfoxides,[13,14] and catalyst-free oxidations of phosphines to their oxides.[15,16] Baeyer−Villiger oxidation is crucial for synthesizing esters from ketones.[17,18]

Aqueous H_2O_2 is a ubiquitous oxidizing agent, but it is not ideal. The major drawback is its abundance of water, which can lead to unwanted secondary reactions. Whenever reagents are not water-soluble the oxidation reactions have to be performed in a biphasic system, slowing rates and requiring phase separations later. Water-free formulations of H_2O_2 such as urea hydrogen peroxide (UHP)[19,20] and peroxocarbonates[21] are used, but they are not very soluble in organic solvents. More promising are the previously described perhydrates.[22,23] Peroxoborates are industrially important oxidants with a world production of more than 550 000 tons per year.[24] Peroxoborates have recently been applied, for example, for selective sulfide oxidation,[25] the stereodefined synthesis of lactones,[26] and the synthesis of flavones.[27] Peroxides like $(Me_3SiO)_2$ and $(CH_3)_2C(OO)$ (DMDO) are also in use; however, their synthesis and storage are not trivial.[28]

Phosphine oxides are important synthetic targets and intermediates.[29−31] For example, they are applied for Mitsunobu reactions[32] and recently attracted attention as redox-free Mitsunobu organocatalysts.[33] On the other hand, phosphine oxides are coproducts of Appel and Wittig reactions and unwanted byproducts of phosphine chemistry in general, especially when catalysts are immobilized on oxide supports via phosphine linkers.[34−37] They are applied to probe surface acidities[38,39] and receive attention in the decomposition of

Received: July 14, 2020
Published: August 31, 2020

https://dx.doi.org/10.1021/acs.inorgchem.0c02087
Inorg. Chem. 2020, 59, 13719−13732

warfare agents.[40] From an analytical point of view, phosphine oxides display interesting mobilities on surfaces that have recently been studied by solid-state NMR.[41−43]

One of the most important features of phosphine oxides with respect to this contribution is their ability to form hydrogen bonds with a variety of different donors. For example, phenols are used in combination with phosphine oxides to create extended hydrogen-bonded networks,[44−46] and hydrogen bonding with naphthol,[47] sulfonic acids,[48] and water has been reported.[43,48−50] Silanols and chloroform crystallize as hydrogen-bonded assemblies.[51] Besides single crystal X-ray diffraction, ^{31}P solid-state NMR spectroscopy has been applied as a powerful method to analyze the hydrogen bonding characteristics of diverse P(V) species.[41−43,52,53]

Combining the unique potential of phosphine oxides to form well-defined hydrogen bonding motifs with the quest for superior oxidizing agents, we recently discovered two new types of stabilized peroxides. The Hilliard hydrogen peroxide adducts $(R_3PO{\cdot}H_2O_2)_2$ (R = alkyl, aryl) can be obtained by combining phosphines with aqueous H_2O_2.[15,50,54,55] In the presence of ketones (R′COR″), di(hydroperoxy)alkane adducts $R_3PO{\cdot}(HOO)_2CR'R''$ (R, R′, R″ = alkyl, aryl) are generated (Ahn adducts).[54−57] For the sake of brevity, we will refer to Ahn adducts in the following.

Preliminary research has already indicated that Ahn adducts are solid and soluble in organic solvents and that they exhibit well-defined structure and composition.[54−57] They are easy to synthesize and convenient to administer to reaction mixtures. No traces of potentially dangerous triacetone triperoxide (TATP) has ever been found in any preparation. Ahn adducts selectively and instantaneously oxidize phosphines to phosphine oxides, without insertion of oxygen into any P−C bond.[54−57] The additional merit of oxidations that can be performed in nonaqueous media has been demonstrated by the clean synthesis of the water-sensitive $Ph_2P(O)P(O)Ph_2$.[56] The ease of stoichiometric administration of the solid Ahn oxidizers has furthermore been demonstrated by the selective oxidation of sulfides into sulfoxides that is performed without overoxidation to sulfones.[55,56] The Baeyer−Villiger oxidation of cyclic ketones has been studied with representative Ahn adducts, and lactones have been obtained selectively, without adverse hydrolysis or polymerization, while only a trace amount of acid catalyst was needed.[57]

In this contribution, we broaden the basis of known di(hydroperoxy)cycloalkane adducts of triarylphosphine oxides with different steric demands and electronic properties. Their solid-state characteristics are explored by single crystal X-ray diffraction, IR, and Raman spectroscopy. In solution, ^{31}P NMR and natural abundance ^{17}O NMR serves to characterize all Ahn adducts. Furthermore, a systematic study has been undertaken to quantify the association of the Ahn adducts, i.e., the strength of the hydrogen bonding of di(hydroperoxy)cyclohexane and -heptane to the phosphine oxides with different electronic and steric properties. This study is supported by diffusion ordered spectroscopy (DOSY).[58,59] Hereby, ^{1}H DOSY[60] that tracks the movements of both hydrogen-bound peroxides and phosphine oxide carriers is the most favorable method. The obtained Stokes diameters reveal the association of the adducts. Quantitative data gained with dynamic ^{31}P VT NMR spectroscopy yield for the first time the activation energies for the exchange of phosphine oxide carriers by the di(hydroperoxy)cycloalkanes.

2. RESULTS AND DISCUSSION

2.1. Synthesis and Characterization. In order to broaden the range of available di(hydroperoxy)cycloalkane adducts (Ahn adducts) of triarylphosphine oxides, and further explore diverse analytical methods for their characterization, the triarylphosphine oxides **1** and **2**, and the adducts **3**−**6** have been synthesized (Figure 1). The syntheses of **1** and **2** were

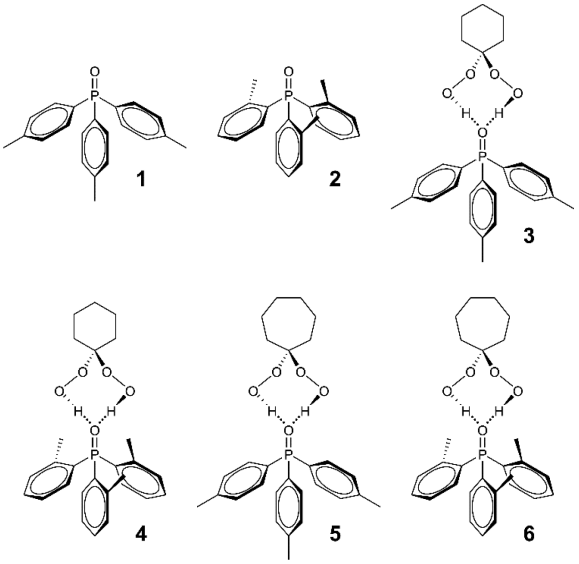

Figure 1. Phosphine oxides **1** and **2** and their Ahn adducts (di(hydroperoxy)alkane adducts) **3**−**6**.

straightforward by combining dichloromethane solutions of the corresponding phosphines with 35% aqueous hydrogen peroxide, as described earlier.[15,61] The Ahn adducts **3**−**6** were obtained with stoichiometrically precise compositions by combining **1** and **2** with di(hydroperoxy)cyclohexane and di(hydroperoxy)cycloheptane. The latter have been synthesized according to a literature procedure[62] and used for the adduct formation as soon as possible. The adducts were obtained pure and in high yields of 74 to 89% without elaborate purification operations.

All adducts **3**−**6** proved to be stable mechanically and thermally and their melting points or ranges could be determined. The characterization of the adducts was furthermore facilitated by their readiness to crystallize in large single crystals with dimensions in the centimeter range (Figure 2). Besides the single crystal X-ray structures, the IR and Raman spectroscopic data are reported of the solid polycrystalline materials. The ^{31}P solution NMR data are in

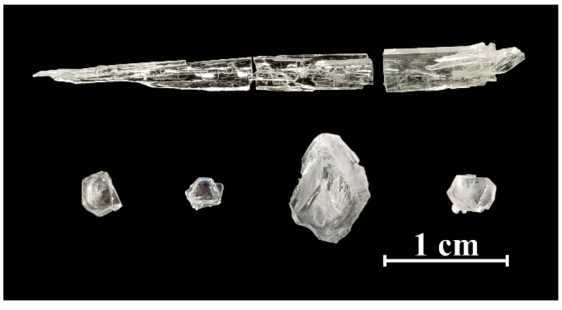

Figure 2. Representative single crystals of **3** (top) and **6** (bottom).

https://dx.doi.org/10.1021/acs.inorgchem.0c02087
Inorg. Chem. 2020, 59, 13719−13732

agreement with earlier results on Ahn adducts. Additionally, due to the high solubility of all adducts, high-quality natural abundance ^{17}O NMR spectra of **3**–**6** could be obtained for the first time with well-resolved signals for the di(hydroperoxy)-cycloalkane and P═O oxygen nuclei. Competition and dynamic VT ^{31}P NMR investigations, as well as ^{1}H DOSY experiments elucidate the dissociation of the adducts in solution. The Gibbs energies of activation $\Delta G^{\ddagger}$, as well as the enthalpy $\Delta H^{\ddagger}$ and entropy of activation $\Delta S^{\ddagger}$ for these dynamic processes, could be determined.

2.2. X-ray Crystallography. All Ahn adducts **3**–**6** crystallize readily in large colorless specimens of high quality (Figure 2). Since Ph_3PO functions as a crystallization aid for amines,[63] it is assumed that the triarylphosphine oxide moieties are most probably responsible for the ease of crystallization of the adducts. The single crystal X-ray structure of the neat phosphine oxide **1** has been obtained for comparison with the adduct structures (Figure 3). In contrast to $^{n}Bu_3P$═O,[15]

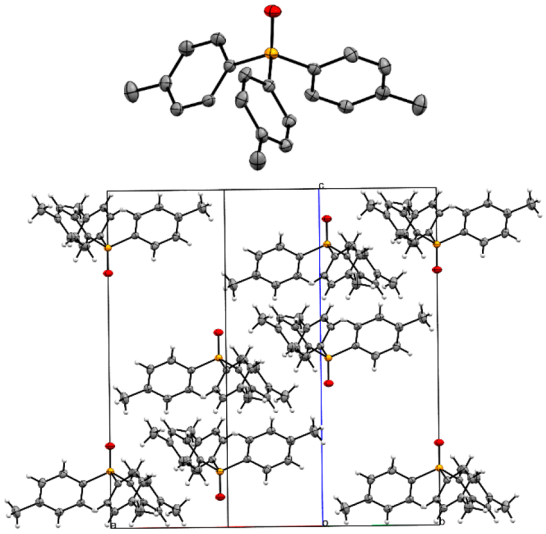

Figure 3. One molecule (top) and unit cell (bottom) of the single crystal X-ray structure of *p*-Tol_3PO (**1**).

where the P═O groups are aligned in the same direction and the molecules are stacked on top of each other, the arrangement of **1** in the crystal lattice is dominated by the *p*-Tol substituents. The substituents of the phosphine oxide molecules face each other, while the P═O groups point in opposite directions (Figure 3). This motif has also been described recently for secondary and tertiary alkylphosphine oxides.[42]

The single crystal X-ray structures of the Ahn adducts **3**–**6** are displayed in Figures 4–7. The relevant data are summarized in Tables 1 and 2. Each adduct assembly of **3**–**6** incorporates two geminal hydroperoxy groups hydrogen-bonded to the oxygen atom of one P═O group. Therewith, the X-ray structures confirm the well-defined adduct composition of one di(hydroperoxy)cycloalkane moiety per phosphine oxide molecule. As previously communicated for other Ahn adducts,[54−57] the crystal lattices of **3**–**6** are assembled by units of two adduct assemblies that are arranged in opposite directions (Figures 4–7). The steric ease of packing two adducts is nicely visible for **3** (Figure 4). The sterically compact nature of these double assemblies explains the ease of crystallization of all Ahn adducts.

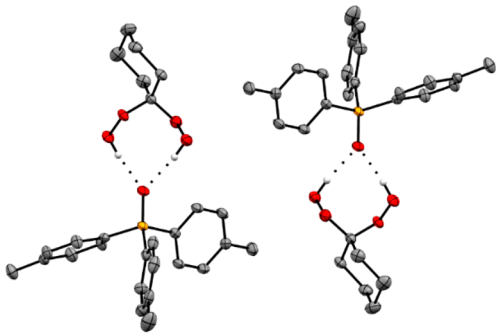

Figure 4. Single crystal X-ray structure of *p*-$Tol_3PO{\cdot}(HOO)_2C(CH_2)_5$ (**3**).

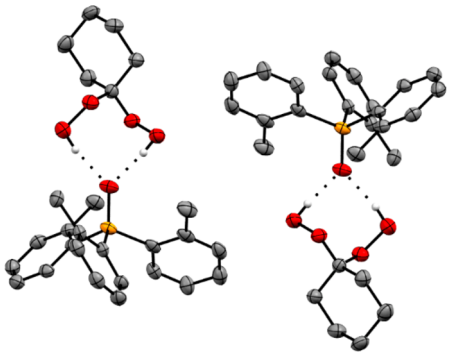

Figure 5. Single crystal X-ray structure of *o*-$Tol_3PO{\cdot}(HOO)_2C(CH_2)_5$ (**4**).

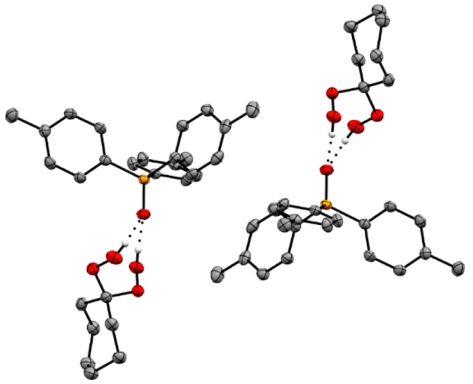

Figure 6. Single crystal X-ray structure of *p*-$Tol_3PO{\cdot}(HOO)_2C(CH_2)_6$ (**5**).

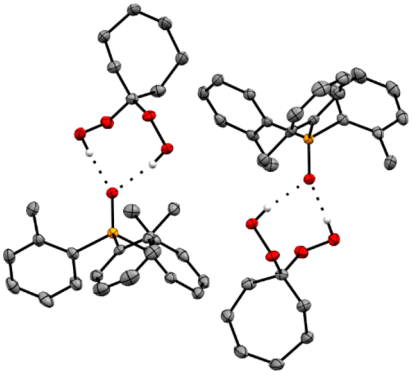

Figure 7. Single crystal X-ray structure of *o*-$Tol_3PO{\cdot}(HOO)_2C(CH_2)_6$ (**6**).

https://dx.doi.org/10.1021/acs.inorgchem.0c02087
Inorg. Chem. 2020, 59, 13719−13732

Table 1. P═O Bond Lengths (Å), Differences Δ(P═O) between the P═O Bond Lengths of the Ahn Adducts 3−6 and the Corresponding Neat Phosphine Oxides 1 and 2 (Å), and the O···H and Oxygen−Oxygen Distances of the Hydrogen Bonds O···H−O (Å) of the Adducts 3−6

species	P═O bond length (Å)	Δ(P═O) (Å)	O···H distance (Å)	O···H−O Distance (Å)
1	1.4885(17)[60]			
2	1.478(2)/ 1.481(2)[61]			
3	1.5047(10)	0.0162	1.862/1.920	2.7038(15)/ 2.7579(14)
4	1.4992(17)	0.0212/ 0.0182	1.842/1.881	2.686(2)/ 2.720(3)
5	1.5031(11)	0.0146	1.842/1.951	2.6889(17)/ 2.7849(17)
6	1.5014(11)	0.0234/ 0.0204	1.856/1.908	2.7057(16)/ 2.7245(16)

Table 2. Dihedral Angles (deg) of the Phosphine Oxides 1 and 2 and the Ahn Adducts 3−6

species	O···O−O−C	C−C−P═O
1		39.77(12)
2		40.8(3)/42.6(3)/53.4(3)
		35.3(3)/47.3(3)/48.6(3)[a,61]
3	92.44(9)/94.42(9)	1.69(14)/7.15(13)/70.83(13)
4	91.17(15)/94.44(15)	36.3(4)/49.2(2)/53.1(X2)
5	90.85(11)/95.45(11)	1.35(16)/3.31(15)/70.64(15)
6	89.25(10)/96.23(10)	42.0(2)/48.96(14)/52.12(14)

[a]Two independent molecules in the asymmetric unit.[61]

The P═O bonds in the adducts **3−6** are all elongated as compared to the neat phosphine oxides (Table 1). The differences range between 0.0162 and 0.0234 Å. Obviously, the hydrogen bonding of the di(hydroperoxy)cycloalkane moieties weakens the P═O bonds and therewith lengthens them. This result is corroborated by IR spectroscopy (see below). The lengthening of the P═O bonds is more substantial for the adducts with *ortho* methyl substituents (**4**, **6**) at the phenyl groups than for those with *para* methyl substituents (**3**, **5**). Since the X-ray structures do not indicate any steric crowding due to the substituents in the *ortho* positions, it is assumed the electronic effects are responsible for this difference in the bond lengthening feature.

The presence of strong hydrogen bonds in all adducts is corroborated by the short O···H distances (Table 1). All O···H distances in **3−6** are within the range of 1.842 to 1.951 Å (Table 1). Typically, hydrogen bonds exhibit O···H distances of 1.85 to 1.95 Å.[65] Additionally, the O···H−O distances of **3−6** have been determined using the single crystal X-ray data. These O···H−O distances represent another indicator for the formation of hydrogen bonds.[66] All values lie within the range of 2.686 to 2.7849 Å (Table 1). This again confirms strong hydrogen bonding, as most of the values are even smaller than the recognized range of 2.75 to 2.85 Å for O···H−O distances in hydrogen bonds.[66]

Next, we analyzed the dihedral angles O···O−O−C in **3−6** (Table 2). Interestingly, one of the hydrogen bridges each in **3−6** displays a dihedral O···O−O−C angle between 89.25° and 92.44°. This is close to the value of 90.2(6)° found for solid H_2O_2. The other hydrogen bridge in each of the adducts **3−6** obviously has to accommodate the packing in the crystal lattice and is more distorted. These dihedral angles assume values within a remarkably narrow range from 94.42° to 96.23° (Table 2).

The cyclohexane and cycloheptane rings show the characteristic chair (**3**, **4**) and boat (**5**, **6**) conformations, respectively. Recently, a conformational analysis of Ph_3P═O has been undertaken using theoretical calculations.[67] According to the theory, the energetic minima of the dihedral angle C−C−P═O should be ±33° or ±25° of 0° or 180°, depending on the method used for the calculations. The experimental distribution of dihedral angles in Ph_3P═O containing metal-free compounds is concentrated in the regions (±15−30°) on either side of 0° and 180°.[67] Since **1−6** are the perfect candidates to test the theory, this research sparked our interest in the dihedral C−C−P═O angles (Table 2). The values in Table 2 indicate that the methyl groups in the *ortho* positions lead to massive deviations from theory and the experimental distribution due to their steric impact in **2**, **4**, and **6**. The phenyl groups are rotated out of the positions of energetic minima that the phenyl groups in Ph_3P═O would assume and display larger dihedral C−C−P═O angles. For **3** and **5**, with the methyl substituents in the *para* positions, the theory and experimental dihedral angle distributions are closer. Two of the three *p*-Tol groups for each, **3** and **5**, lie within the expected range with values from 1.35° to 7.15°. But the third dihedral angle deviates for **3** and **5**, with 70.83° and 70.64°, respectively. Interestingly, different patterns for the dihedral angles C−C−P═O have been observed for the Hilliard adducts ((p-Tol_3P═O·H_2O_2)$_2$, 9.14°/27.26°/81.04°; (o-Tol_3P═O·H_2O_2)$_2$, 46.82°/47.07°/55.35°).[50]

2.3. ^{31}P NMR Spectroscopy. The Ahn adducts **3−6** are highly soluble in organic solvents (see also below).[54−57] Therefore, the ^{31}P NMR spectra can be recorded with just a few scans. A capillary with neat, liquid $ClPPh_2$, centered within the NMR tubes, conveniently serves as a standard. The ^{31}P chemical shifts of the adducts **3−6** show increased values as compared with those of the corresponding phosphine oxides **1** and **2** (Table 3). The trend of the adduct chemical shifts

Table 3. ^{31}P NMR Chemical Shifts of 1-6 in $CDCl_3$ and the Differences of the Chemical Shift Values Δδ(^{31}P) between the Adducts 3−6 and Their Corresponding Phosphine Oxides 1 and 2

species	δ(^{31}P) (ppm)	Δδ(^{31}P) (ppm)
1	29.28	
2	37.51	
3	34.76	5.48
4	42.47	4.96
5	32.51	3.23
6	39.95	2.44

consists of a downfield shift between 2.44 and 5.48 ppm, corroborating earlier results on different Ahn adducts.[54−57] This downfield shift can be explained by the hydrogen bonds to the di(hydroperoxy)cycloalkane moieties, which lead to deshielding of the ^{31}P nuclei. The latter can be attributed to the electron density being drawn toward the oxygen atom in the P═O group. This is why the chemical shift values of Ahn[54−57] and hydrogen peroxide adducts[50] are generally higher than the δ(^{31}P) of the parent phosphine oxides.

In contrast to the ^{31}P chemical shifts, the changes of the ^{1}H and ^{13}C NMR data when forming the Ahn adducts from the phosphine oxides are minimal. This can be seen, for example,

https://dx.doi.org/10.1021/acs.inorgchem.0c02087
Inorg. Chem. 2020, 59, 13719−13732

by comparing the $\delta(^{13}C)$ and $J(^{31}P-^{13}C)$ values of **1** with those of **3**.

2.4. ^{17}O NMR Spectroscopy. ^{17}O NMR poses more challenges than routine ^{31}P NMR spectroscopy. The Larmor frequency of ^{17}O lies within an easily accessible range, but the natural abundance of this nucleus is only 0.037%, which is about half of the value for deuterium. The nuclear spin of the ^{17}O isotope is $I = 5/2$, and therewith it is quadrupolar in nature. The quadrupole moment $Q = -2.6 \times 10^{-26}$ is moderate,[68] which leads to ^{17}O resonances that are typically broader than 100 Hz for species with unsymmetric electronic surroundings of the ^{17}O nucleus. Most ^{17}O NMR investigations have been carried out with isotopically enriched samples to facilitate the measurements. Examples include studies of organic peroxides[69] and alkyl hydrotrioxides.[70] Furthermore, the peroxide binding to the active center of an enzyme[71] and polymer degradation mechanisms have been studied using ^{17}O NMR.[72] Enriched samples were also applied for studying polymorphs of triphenylphosphine oxide[73] and the hydrogen bonding in carboxylic acids by ^{17}O solid-state NMR.[74]

Fortunately, the fast quadrupolar relaxation[68] allows for the scans to be administered in rapid succession, and compounds without isotopic enrichment but with sufficient solubility in nonaqueous liquids are accessible to natural abundance ^{17}O NMR.

The adducts **3**–**6** are highly soluble in organic solvents (see below). Especially their excellent solubility in benzene is advantageous because it allows the measurement of very concentrated samples in a solvent that can be heated up to reduce its viscosity. The lower viscosity of benzene at elevated temperatures shortens the correlation times of the dissolved adducts and therefore diminishes the halfwidths of the quadupolar ^{17}O NMR resonances.[68]

A representative ^{17}O NMR spectrum is shown in Figure 8. The ^{17}O NMR data of the Ahn adducts **3**–**6** and the original

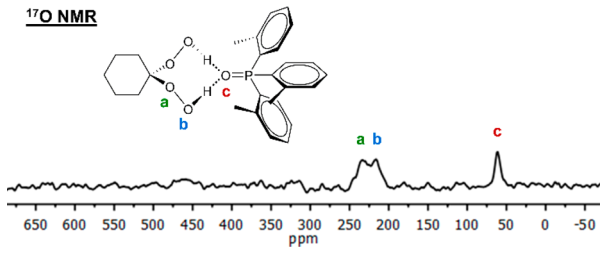

Figure 8. Natural abundance ^{17}O NMR spectrum of *o*-$Tol_3PO\cdot(HOO)_2C(CH_2)_5$ (**4**) in benzene, recorded at 70 °C.

phosphine oxides **1** and **2** are summarized in Table 4. The spectrum in Figure 8 shows the three expected signals of **4**. Although the halfwidths are substantial and of triple digit magnitude in units of Hz, most resonances are resolved because of the large chemical shift dispersion of ^{17}O. The oxygen nucleus of the P═O group resonates at 61.36 ppm, which is well within the region for phosphine oxides (Table 4).[50] The two ^{17}O NMR signals of the di(hydroperoxy)-cycloalkane moiety are found at 234.9 and 216.3 ppm. The signal assignment given in Figure 8 is based on a comparison with $\delta(^{17}O)$ of $^{t}BuOO^{t}Bu$ (269 ppm) and $^{t}BuOOH$ (243 ppm for C–O, 208.5 ppm for O–H).[69]

It is important to note that the Ahn adducts do not decompose during the measurement at 70 °C. No signals

Table 4. ^{17}O NMR Chemical Shifts $\delta(^{17}O)$ (Signal Halfwidths $\Delta\nu_{1/2}$ (Hz)) of the Phosphine Oxides 1 and 2, and the Ahn Adducts 3–6 in C_6H_6 at 70 °C

	$\delta(^{17}O)$ (ppm) of bound $R(OOH)_2$ ($\Delta\nu_{1/2}$ (Hz))		
adduct	C–O	O–H	$\delta(^{17}O)$ (ppm) of P═OX group ($\Delta\nu_{1/2}$ (Hz))
1			50.35[a] (235)
2			66.16 (379)
3	229.3 (979)	217.9(516)	48.37 (644)
4	234.9 (815)	216.3 (1017)	61.36 (545)
5	246.2[b] (820)	246.2[b] (820)	48.89 (611)
6	188.9[b] (391)	188.9[b] (391)	63.73 (441)

[a]Signal is split into a doublet with $^{1}J(^{31}P-^{17}O)$ = 129.9 Hz. [b]C–O and O–H signals are not resolved.

corresponding to the decomposition products free water (0 ppm) or water hydrogen-bound to phosphine oxide,[50] hydrogen peroxide (179.3 ppm),[69,71] or any of the parent ketones[68] have been found.

The $\delta(^{17}O)$ of the P═O groups of the Ahn adducts **3**–**6** are found within the range of 48.37 to 63.73 ppm (Table 4), in accordance with the range for the hydrogen peroxide (Hilliard) adducts of the same phosphine oxides (46.60 to 60.04 ppm),[50] and with other compounds incorporating phosphorus–oxygen double bonds.[75] As compared to the $\delta(^{17}O)$ of the P═O group of **1** (50.35 ppm; Table 4), the chemical shift for the oxygen nucleus of Ph_3P═O in $CDCl_3$ has been reported as 43.3 ppm.[76] The deviation from this value for **1** and the variation of the $\delta(^{17}O)$ for the P═O group in **2** reflects the presence of substituents at the aromatic rings, and the change of the solvent, since the solvent dependence of ^{17}O NMR chemical shifts can be substantial.[78]

Comparing the $\delta(^{17}O)$ of the P═O groups in the adducts **3**–**6** with those of the corresponding phosphine oxides **1** and **2** measured in the same solvent, benzene, shows that hydrogen bonding leads to a slight but consistent upfield shift of the signals, amounting to 1.98 (**1**/**3**), 1.46 (**1**/**5**), 4.80 (**2**/**4**), and 2.43 (**2**/**6**) ppm (Table 4). A similar upfield shift had been observed for the Hilliard adducts earlier.[50] This result can be interpreted in terms of the electron density around the oxygen nucleus being increased by the pull of electrons from the aromatic rings toward oxygen and the hydrogen bond. This leads to a shielding of the ^{17}O nucleus and the observed upfield shift. Regarding the ^{17}O NMR signals of the hydrogen-bonded di(hydroperoxy)cycloalkane moieties in **3**–**6**, comparisons with literature values are limited to the case of $^{t}BuOOH$ mentioned above[69] because the data displayed here are the first for Ahn adducts.

The $\Delta\nu_{1/2}$ values are in most of the cases presented larger for the hydroperoxy oxygen nuclei than for oxygen in the P═O groups (Table 4). The halfwidth $\Delta\nu_{1/2}$ of the ^{17}O phosphine oxide signal of **1** is even small enough to reveal its splitting into a doublet with $^{1}J(^{31}P-^{17}O)$ = 129.9 Hz. This value is in accordance with that of Ph_3P═O in $CDCl_3$ (160 Hz).[76] The correlation time of the hydrogen-bonded di(hydroperoxy)-cycloalkane moieties and the carrier phosphine oxides has to be the same, as the adduct assembly moves in unison. Therefore, the larger halfwidths of the peroxy oxygen signals compared with the P═O resonance must have its origin in a greater electronic asymmetry.

https://dx.doi.org/10.1021/acs.inorgchem.0c02087
Inorg. Chem. 2020, 59, 13719–13732

2.5. DOSY NMR Spectroscopy. The adducts **3**−**6** feature di(hydroperoxy)cycloalkane moieties hydrogen-bonded to phosphine oxides in a 1:1 ratio in the solid state. Although the affinity of the components in the solids is obvious, no information about the dissociation of **3**−**6** in a solvent has been reported so far. In contrast to the Hilliard adducts, for the Ahn adducts each assembly of two components is held together by two intramolecular hydrogen bonds.

While a certain degree of dissociation has been found for the Hilliard adducts,[50] no prediction is feasible for the Ahn adducts in solution. In order to get insight into this issue, we sought to employ diffusion-ordered NMR spectroscopy (DOSY) to probe the hydrogen bond association in **3**−**6**.[58,59] For this purpose, the straightforward ^{1}H DOSY experiments have been employed.[60] The obtained Stokes diameters can then be compared with the expected diameters of **1**−**6** based on their maximal extensions in the X-ray structures. Although the associates **3**−**6** are not entirely spherically symmetric, but somewhat elongated (Figures 4−7), the resulting values for the Stokes diameters should lie within an error margin of ±2 Å. For the phosphine oxides **1** and **2**, larger deviations of the Stokes diameters from the largest H···H distances have to be acknowledged because their shape is more of an umbrella type than spherical (Figure 3), which increases their resistance toward diffusion. The Stokes diameters of the adducts **3**−**6** and the corresponding phosphine oxides **1** and **2** have been compared to the maximal sizes of the species, as defined by the largest H···H distances in their X-ray structures (Table 5).

Table 5. Stokes Diameters of the Phosphine Oxides 1 and 2, and the Ahn Adducts 3−6 Obtained from ^{1}H DOSY Measurements in C_6D_6[a]

species	Stokes diameter (Å)	maximal H···H distance (Å)	difference (Å)
1	15.1	13.677	1.4
2	14.5	11.867	2.6
3	17.4	16.299	1.1
4	17.0	15.349	1.7
5	17.9	16.942	1.0
6	15.4	15.880	0.5

[a]The maximal H···H distances were obtained from the atomic positions in the X-ray structures of the adduct assemblies **3**−**6** and include 2 times the van der Waals radius of H. The last column reports the differences between the Stokes diameters and the maximal H···H distances in **1**−**6**.

Indeed, the obtained Stokes diameters for the umbrella-shaped phosphine oxides are somewhat larger than the structural data would imply. However, the values are still within the error margins for monomers, and the presence of stacks of phosphine oxides, as found for example, in solid ^{n}Bu$_3$PO,[15] can be excluded in solution. For the Ahn adducts **3**−**6**, the Stokes diameters fit very well the assumption that in solution the 1:1 adduct assemblies as a whole, consisting of the phosphine oxide and di(hydroperoxy)cycloalkane moiety, as found in the solid state, are diffusing through the solution in unison.

The DOSY result that the adducts **3**−**6** do not completely dissociate into R_3PO and $(HOO)_2C(CH_2)_{5/6}$ moieties is also corroborated by the fact that the adducts show solubilities in most organic solvents that are different from those of the parent phosphine oxides (see solubilities below).

2.6. Dynamic NMR Spectroscopy of Ahn Adducts. *2.6.a. Competition Experiments.* The DOSY experiments described above prove that the adducts **3**−**6** diffuse through solution as hydrogen-bonded assemblies with the phosphine oxides and di(hydroperoxy)cycloalkane components in a 1:1 ratio. Therefore, most of the time, the assemblies stay together.

However, this does not mean that an exchange between the components could not happen that is fast as compared to the DOSY NMR time scale. In other words, the peroxy moiety could jump from one phosphine oxide carrier to the next. In order to probe this possibility, competition experiments have been performed, as depicted for one representative example in Scheme 1. Hereby, the potential migration of the di-

Scheme 1. Equilibrium of a 1:1 Mixture of *p*-Tol$_3$PO·(HOO)$_2$C(CH$_2$)$_5$ (3) and Cy$_3$PO (7) with the Products *p*-Tol$_3$PO (1) and Cy$_3$PO·(HOO)$_2$C(CH$_2$)$_5$ (8)

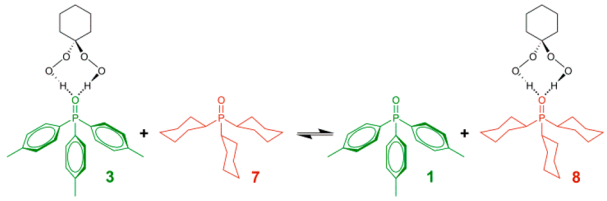

(hydroperoxy)cycloalkane moiety from one phosphine oxide carrier to another one of the same (Scheme 2) or of a different sort (Scheme 1) is monitored.

Scheme 2. Exchange Equilibrium for a 1:1 Mixture of *o*-Tol$_3$PO (2) and *o*-Tol$_3$PO·(HOO)$_2$C(CH$_2$)$_5$ (4)

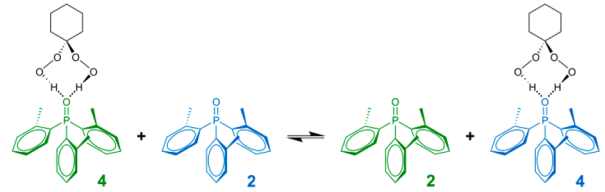

In practical terms, an equimolar excess of the same or a different phosphine oxide is offered to the solution of an adduct, and the resulting ^{31}P NMR spectrum is evaluated. For example, when adduct **3** is combined with an equal amount of the phosphine oxide Cy$_3$PO (**7**), the phosphine oxide **1** could be liberated completely, and adduct **8** could be formed quantitatively (Scheme 1). Alternatively, no changes could occur, in which case **3** and **7** would persist as the only species in the mixture. Of course, there could also be an equilibrium with all four entities, **1**, **3**, **7**, and **8**, present in an equilibrium that is not shifted entirely to the right or left side.

In order to quantitatively probe the ability of the peroxy moiety to migrate, exact amounts of adducts and competing phosphine oxides have been weighed in. For obtaining precise ^{31}P NMR chemical shifts, capillaries containing pure liquid Ph$_2$PCl were centered in the NMR tubes. In a first step, the $\delta(^{31}P)$ of the pure phosphine oxides **1**, **2**, and **7** as well as all adducts were determined in benzene (Table 6). The latter was chosen as a nonprotic and unpolar solvent to avoid complications due to exchange with solvent molecules. The representative examples displayed in Figure 9 will be discussed here, the NMR spectra and all data of the other competition

https://dx.doi.org/10.1021/acs.inorgchem.0c02087
Inorg. Chem. 2020, 59, 13719−13732

Table 6. ^{31}P NMR Chemical Shifts Obtained in Competition Experiments When the Ahn Adducts 3−6 Are Combined with Equal Amounts of the Phosphine Oxides 1, 2, and 7 in Benzene[a]

		$\delta(^{31}P)$ (ppm) of adduct after adding an equal amount of the phosphine oxide		
adduct	$\delta(^{31}P)$ (ppm)	*p*-Tol_3PO (**1**)	*o*-Tol_3PO (**2**)	Cy_3PO (**7**)
3	33.06	29.63	30.56	27.02
4	41.57	38.17	38.98	36.50
5	32.48	29.34	30.24	26.60
6	40.11	37.35	38.05	36.03

[a]The $\delta(^{31}P)$ of the phosphine oxides in benzene are 25.53 ppm (**1**), 37.71 ppm (**2**), and 45.99 (**7**).

experiments are provided for in Tables 6 and 7 and in the Supporting Information.

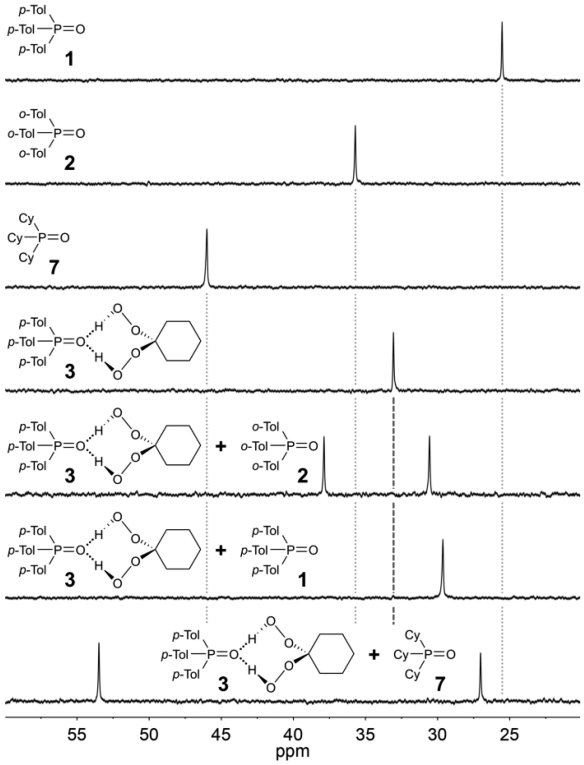

Figure 9. Competition experiments: ^{31}P NMR spectra of the phosphine oxides *p*-Tol_3PO (**1**), *o*-Tol_3PO (**2**), and Cy_3PO (**7**), the pure adduct *p*-$Tol_3PO{\cdot}(HOO)_2C(CH_2)_5$ (**3**), and 1:1 mixtures of **3** with the phosphine oxides **1**, **2**, and **7** in benzene at ambient temperature.

Table 7. ^{31}P NMR Chemical Shift Differences between the Adducts 3−6 and the $\delta(^{31}P)$ That Result When an Equal Amount of 1, 2, and 7 Is Added to Their Benzene Solution

	$\Delta\delta(^{31}P)$ = [$\delta(^{31}P)$ of adduct] − [$\delta(^{31}P)$ of adduct in 1:1 mixture with phosphine oxide]		
adduct	*p*-Tol_3PO (**1**)	*o*-Tol_3PO (**2**)	Cy_3PO (**7**)
3	3.43	2.50	6.04
4	3.40	2.59	5.07
5	3.14	2.24	5.88
6	2.76	2.06	4.08

When an equal amount of **1** is added to a solution of **3**, a sharp signal is obtained at 29.63 ppm, which is about halfway in between the chemical shifts of **1** (25.53 ppm) and **3** (33.06 ppm; Figure 9, Table 6). The position and small halfwidth of the one resulting resonance indicate that the exchange of the di(hydroperoxy)cycloalkane moiety between the phosphine oxide carriers is fast on the ^{31}P NMR time scale at room temperature. Very slow exchange, with **1** and **3** coexisting in solution, would have allowed both signals of the phosphine oxide and adduct to be visible and sharp in the spectrum. A moderate exchange rate on the time scale of ^{31}P NMR would have resulted in individual broad lines. Analogous results were obtained for 1:1 mixtures of **1** and **5**, **2** and **4**, and **2** and **6** (Table 6 and Supporting Information).

Next, we sought to investigate the relative affinities of di(hydroperoxy)cyclohexane and di(hydroperoxy)-cycloheptane to *p*-Tol_3PO (**1**), *o*-Tol_3PO (**2**), and Cy_3PO (**7**). The affinities were assessed by experiments probing the competition between the adducts **3**−**6** and different phosphine oxides. For example, an equal amount of Cy_3PO (**7**) has been added to *p*-$Tol_3PO{\cdot}(HOO)_2C(CH_2)_5$ (**3**; Figure 9, bottom spectrum, Table 6). In this case, an equilibrium mixture is obtained. The original signal of **3** at 33.06 ppm is shifted upfield to 27.02 ppm, but not quite reaching the chemical shift of pure **1** (25.53 ppm). This indicates that **3** lost some but not all of the hydrogen-bonded di(hydroperoxy)cyclohexane. At the same time, **7** undergoes a downfield shift from originally 45.99 ppm to 53.48 ppm, which proves the formation of a certain amount of $Cy_3PO{\cdot}(HOO)_2C(CH_2)_5$ (**8**). Overall, the mixture contains **3** and **7**, as well as **1** and **8**, so the equilibrium outlined in Scheme 1 does not pivot entirely to the right or left side.

As the next step, we sought to estimate the affinities of the peroxy moieties to the different phosphine oxides in a qualitative manner. For this purpose, we contemplated the ^{31}P chemical shift changes that all adducts **3**−**6** undergo when equimolar amounts of the phosphine oxides **1**, **2**, and **7** are added (Table 7). When **7** was added to the adducts **3**−**6**, their signals shifted 4.08−6.04 ppm upfield. Adding **1** or **2** led to upfield shifts of 2.76−3.43 ppm and 2.06−2.59 ppm, respectively. The shift differences are largest for **7** and smallest for **2**. Therefore, the relative affinities of both di(hydroperoxy)-cycloalkanes with respect to hydrogen bonding are increasing from **2** over **1** to **7**.

2.6.b. Variable Temperature ^{31}P NMR Experiments. While the competition experiments discussed above served well for gaining some insight into the adduct association in a qualitative manner, in the following a quantitative approach is described.

In order to quantify the dissociation of the Ahn adducts in solution, ^{31}P NMR spectra of 1:1 mixtures of **3**−**6** with their corresponding phosphine oxides **1** and **2**, as despicted for one example in Scheme 2, have been recorded at variable temperatures. At 20 °C, all mixtures show fast exchange of the di(hydroperoxy)cycloalkane moieties between the phosphine oxides, as also described above. Upon cooling, coalescence is reached at about −75 °C (**3**), −70 °C (**5**), −60 °C (**6**), and −50 °C (**4**). At −80 °C, the exchange is slowed down substantially (Figure 10 and Supporting Information). However, the signals are still broad, and therefore the low temperature limit with complete resolution of the adduct and phosphine oxide peaks presumably lies much lower. Fortunately, the ^{31}P NMR spectra of the pure phosphine oxides **1** and **2** and the Ahn adducts **3**−**6** could be recorded

https://dx.doi.org/10.1021/acs.inorgchem.0c02087
Inorg. Chem. 2020, 59, 13719−13732

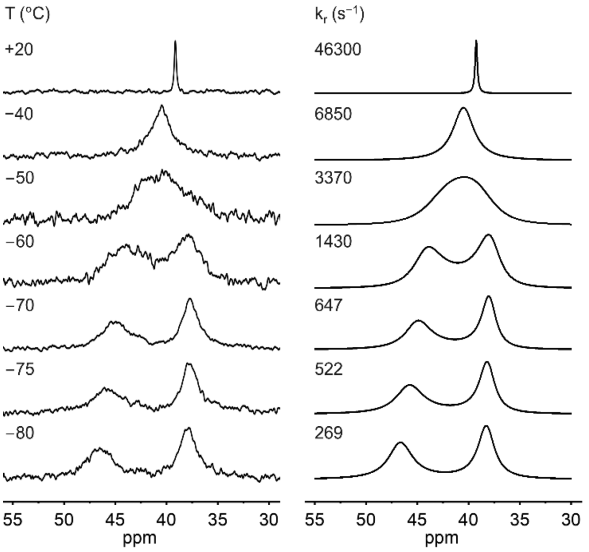

Figure 10. Variable temperature ^{31}P NMR spectra of a 1:1 mixture of *o*-Tol_3PO (**2**) and *o*-$Tol_3PO{\cdot}(HOO)_2C(CH_2)_5$ (**4**) in dichloromethane, recorded at the indicated temperatures (left) and the respective simulations (right).

separately to obtain the precise values for the chemical shifts and line widths at all temperatures (Supporting Information, Table S3). Therefore, a need to reach the low temperature limit did not arise. Simulations[78] were performed using these chemical shifts and line width values, iterating solely on the rate constant of exchange (k_r).

Using the Eyring equation, the Gibbs energy of activation ($\Delta G^{\ddagger}$)[79] values summarized in Table 8 were obtained

Table 8. $\Delta G^{\ddagger}$ Values for the Exchange Reaction of a Di(hydroperoxy)alkane between Two Identical Phosphine Oxides at the Corresponding Temperatures

T (°C)	$\Delta G^{\ddagger}$ (kJ/mol)			
mixture (1:1)	1:3	2:4	1:5	2:6
+20	45.5	45.6	45.6	44.0
−40		39.5		38.0
−50		39.0		38.1
−60	35.5	38.7	36.2	37.8
−70	35.3	38.2	35.5	37.1
−75	34.7	37.5	35.2	36.7
−80	34.4	37.6	35.1	36.5

assuming a transmission coefficient of $\kappa = 1$.[79,80] At 20 °C, these $\Delta G^{\ddagger}$ values range from 44.0 kJ/mol for the pair **2**/**6** to 45.6 kJ/mol for **1**/**5**. At this point, a comparison with similar, well-known scenarios is interesting. For example, the energy barrier of a hydrogen bond breakage in an isolated protein *β*-sheet corresponds to a $\Delta G^{\ddagger}$ of 20 kJ/mol,[81] while the energy needed to initiate a proton transfer in water amounts to 21 kJ/mol.[82] The activation barrier for the transfer of a di(hydroperoxy)cycloalkane from one phosphine oxide to another, identical, one is about twice as large.

The values for the activation enthalpy ($\Delta H^{\ddagger}$) and entropy ($\Delta S^{\ddagger}$) have been obtained from Eyring plots[79] (Figure 11 and Supporting Information) and summarized in Table 9. The pairs **1**/**3** and **1**/**5** with the more tightly hydrogen-bonded *p*-Tol_3PO feature lower enthalpies of activation ($\Delta H^{\ddagger}$) than the mixtures **2**/**4** and **2**/**6**. Considering the hydrogen-bonding of

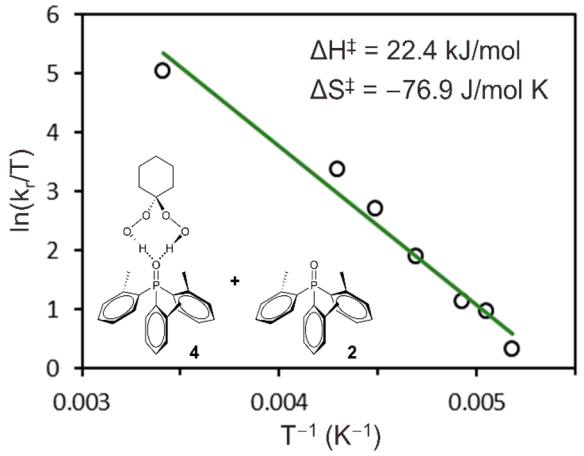

Figure 11. Temperature dependence of the exchange rate constant k_r, depicted as $\ln(k_r/T)$ versus T^{-1}, of a 1:1 mixture of *o*-Tol_3PO (**2**) and *o*-$Tol_3PO{\cdot}(HOO)_2C(CH_2)_5$ (**4**) in dichloromethane.

Table 9. $\Delta H^{\ddagger}$ and $\Delta S^{\ddagger}$ Values for the Exchange Reaction of a Di(hydroperoxy)alkane between Two Identical Phosphine Oxides

mixture (1:1)	1/3	2/4	1/5	2/6
$\Delta H^{\ddagger}$ (kJ/mol)	12.4	22.4	14.0	22.5
$\Delta S^{\ddagger}$ (J/(mol·K))	−112.0	−76.9	−107.0	−71.0

another phosphine oxide molecule during the transition state, the overall number of hydrogen bonds stays the same. Firm hydrogen-bonding with the more basic *p*-Tol_3PO (see IR spectroscopy below) explains the lower enthalpy loss in those transition states as compared to the cases involving *o*-Tol_3PO.

The low entropies of activation ($\Delta S^{\ddagger}$) range from −71.0 J/(mol·K) to −112.0 J/(mol·K) (Table 9). They are close to values observed for highly polar transition states that can be as low as −175 J/(mol·K).[79] The latter are well solvated and thus highly ordered, leading to a very negative entropy of activation. A mostly associated nature of the adducts **3**−**6**, when dissolved in the only moderately polar solvent dichloromethane, can be assumed based, for example, on the DOSY (above) and solubility (below) experiments. Therefore, the negative entropies of activation for **3**−**6** are most probably not caused by a highly ordered solvent shell but by an otherwise highly ordered transition state. This transition state could, for example, be an assembly of the general form $[R_3PO{\cdot}HOOCR_2OOH{\cdot}OPR_3]^{\ddagger}$. The entropies of activation ($\Delta S^{\ddagger}$) of the pairs **1**/**3** and **1**/**5** are more negative than those of **2**/**4** and **2**/**6**. As in the case of $\Delta H^{\ddagger}$ discussed above, this result most probably reflects the stronger hydrogen bonds that di(hydroperoxy)cycloalkanes form with **1** as compared with **2**.

2.7. IR and Raman Spectroscopy. The IR spectra[84] of the Ahn adducts **3**−**6** and the pure phosphine oxides **1** and **2** are in accordance with the ^{31}P NMR spectroscopy results (Table 10). The stretching frequencies and wavenumbers for the P═O groups are 6 to 35 cm^{-1} lower for **3**−**6** as compared to **1** and **2** because the hydrogen bonding of the oxygen atom with the di(hydroperoxy)cycloalkane moieties weakens the double bond. Therefore, less energy is required to excite the stretching mode of the bond in the adducts, the bond order is diminished, and lower wavenumbers are observed. The differences $\Delta\nu$(P═O) are in the range of 6 to 35 cm^{-1}, in accordance with an earlier study of Hilliard H_2O_2 adducts.[50] It

https://dx.doi.org/10.1021/acs.inorgchem.0c02087
Inorg. Chem. 2020, 59, 13719−13732

Table 10. IR Stretching Bands ν(P═O) (cm^{-1}) of the P═O Groups of the Neat Phosphine Oxides 1 and 2 and the Ahn Adducts 3–6.[a] Additionally, the IR Bands ν(O–H) and the Raman ν(O–O) Stretching Bands of 3–6 Are Summarized

species	ν(P═O) (cm^{-1})	$\Delta\nu$(P═O) (cm^{-1})	ν(O–H) (cm^{-1})	ν(O–O) (cm^{-1})
1	1185	0		
2	1158	0		
3	1150	35	3254	866
4	1146	12	3240	863
5	1150	35	3275	873
6	1152	6	3246	868

[a] $\Delta\nu$(P═O) (cm^{-1}) stands for the wavenumber differences between the adducts and the corresponding neat phosphine oxides.

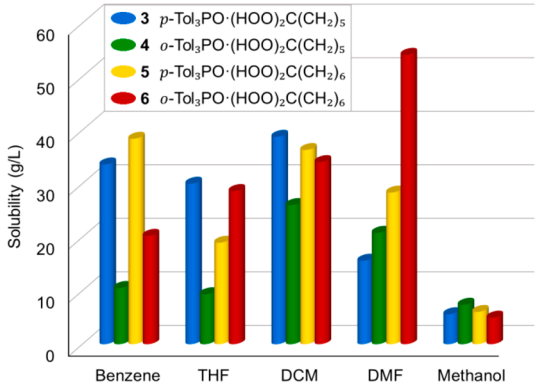

Figure 12. Solubilities of the Ahn adducts 3–6 in selected organic solvents.

should also be noted that hydrogen bonding to **1** leads to a lower ν(P═O) value in both **3** and **5** ($\Delta\nu$(P═O) = 35 cm^{-1}), as compared to bonding to **2** ($\Delta\nu$(P═O) = 6 and 12 cm^{-1}; Table 10). This corroborates the assumption that **1** is hydrogen-bound more firmly to di(hydroperoxy)cycloalkanes, which corresponds well to the results of the activation enthalpy $\Delta H^{\ddagger}$ for the adduct exchange discussed above.

The ν(O–H) stretching bands of the hydrogen-bonded di(hydroperoxy)cycloalkane moieties in **3–6** display wavenumbers of 3240 to 3275 cm^{-1}, which can be clearly distinguished from potential water bands at about 3400 cm^{-1}.[15,83] The hydrogen bonding of the O–H hydrogen atoms to the P═O group weakens the O–H bonds, which leads to lower ν(O–H) wavenumbers.

Due to the favorable symmetry of the adducts **3–6**, the Raman spectra show the O–O stretching bands (Table 10). The intensities of these bands are lower as compared to those from the entirely symmetric Hilliard hydrogen peroxide adducts,[50] but they are still discernible. The ν(O–O) values are found within the narrow range from 863 to 873 cm^{-1}, in agreement with the Raman data of Hilliard adducts,[50] and with theoretically predicted values for $(Ph_3PO{\cdot}H_2O_2)_2$.[84] As expected, due to the bond order of one, the wavenumbers are much lower than those found for O_2 gas (1556 cm^{-1})[85] and O_2^- (1139 cm^{-1}).[86] Basically, the ν(O–O) for hydrogen-bonded di(hydroperoxy)cycloalkanes in **3–6** lies in the region of values for aqueous (99.5%) H_2O_2 (880 cm^{-1})[87] and H_2O_2 vapor (864 cm^{-1}).[88] However, the O–O bonds in **3–6** are still stronger than those in alkali peroxides (736–790 cm^{-1})[89] or the oxidizing agent ^{t}BuOOH (847 cm^{-1}).[90] Overall, the IR and Raman data of **3–6** corroborate the results of the low-temperature ^{31}P NMR experiments.

2.8. Solubilities. From a practical point of view, the most attractive characteristic of the Ahn adducts **3–6** is their high solubility in organic solvents (Figure 12). They are soluble in aromatic solvents like benzene, in polar solvents with electron donation capabilities, such as THF, dichloromethane (DCM), and dimethylformamide (DMF), as well as in protic solvents like alcohols. Interestingly, in contrast to the Hilliard adducts of the same phosphine oxides,[50] the solubilities of all Ahn adducts are lowest in methanol (Figure 12). In fact, the solubilities of **3–6** in methanol are roughly 2 orders of magnitude lower than those of the corresponding Hilliard adducts.[50] The solubilities of the Ahn adducts **3–6** in methanol (5–7 g/L) are also much lower than the solubilities of the corresponding phosphine oxides **1** (25 g/L) and **2** (45 g/L) in this solvent. We assume that, in accordance with the exchange and competition experiments described above, the solvent does not lead to prolonged dissociation of the adducts, and the solubilities obtained (Figure 12) reflect the fact that **3–6** overall have an unpolar character.

Overall, for adducts containing *o*-Tol substituents (**4**, **6**), the solubilities in nonprotic solvents like THF or CH_2Cl_2 are higher for adducts incorporating seven-membered alkyl rings as compared to those with six-membered rings (**3**, **4**). For adducts with *p*-Tol groups, no trend for the dependence on the alkyl ring size is discernible.

The high solubilities of **3–6** in organic solvents are beneficial for many oxidation reactions. For example, the selective oxidations of phosphines to phosphine oxides[54−57] or sulfides to sulfoxides[55,56] can be performed in one organic phase, rendering a biphasic reaction mixture obsolete. Especially in cases where a large amount of water in the aqueous phase could lead to unwanted secondary products, this is advantageous. For example, it has been described previously that cyclic ketones could selectively be oxidized to lactones via Baeyer–Villiger reactions without hydrolysis and polymerization when using Ahn adducts.[57] Whenever all educts are dissolved in one phase, the reactions also proceed faster as compared to processes that only take place at phase boundaries. Furthermore, no phase separations or cumbersome drying procedures for the products are required when reactions with **3–6** are performed in organic solvents. The one water molecule formed per P═O group for **3–6** in cases where all peroxy groups have reacted remains firmly bound to the phosphine oxide carriers and will not interfere with the product or the progress of the reaction. The structures and characteristic data of representative water adducts of phosphine oxides have been reported previously.[43,50] Once the above-mentioned oxidation reactions are complete, the phosphine oxide carriers can easily be removed from the reaction mixtures by precipitating them with hexanes. The phosphine oxides can also be bound to insoluble inorganic supports like silica[34−36] and separated from the supernatant reaction mixtures containing the products by decanting. After recharging with H_2O_2 and ketones, the Ahn adducts of the tethered phosphine oxides can be reused.

2.9. Shelf Lives. The Ahn adducts **3–6** are stable when subjected to dry grinding. They do not react to sudden impacts like hammering. Even when the powders are brought directly into a flame, oxygen is released slowly without any violent audible or visual effect. Furthermore, the adducts can be

https://dx.doi.org/10.1021/acs.inorgchem.0c02087
Inorg. Chem. 2020, 59, 13719–13732

molten without initial decomposition, and oxygen slowly effervesces in tiny bubbles at higher temperatures.

As solids, the adducts **3**−**6** remain oxidatively active over weeks at ambient temperatures and months at low temperatures (Table 11). The oxidative power has been determined by a convenient and standardized *in situ* ^{31}P NMR test.[50,54−57] Hereby, for **3**−**6**, 100% oxidative power corresponds to two active oxygen atoms per P═O group in one adduct assembly. The data show that all adducts can be conveniently handled at ambient temperatures and that they allow storage in a freezer for months. Since the Ahn adducts can be generated also from water adducts of phosphine oxides,[56] old batches can easily be restored to 100% oxidative power by reaction with H_2O_2 and ketones and crystallization.

Table 11. Oxidative Power of the Solids 3−6 after Storage between −13 °C and −18 °C for 250 Days[a]

adduct	residual oxidative power (%)
3	99
4	100
5	80
6	68

[a]100% oxidative power corresponds to two active oxygen atoms per adduct assembly.

3. CONCLUSIONS

The presented studies allow the following generalizations. (a) The composition of all Ahn adducts **3**−**6** is well-defined and reproducible, with one di(hydroperoxy)cycloalkane moiety hydrogen-bonded to one phosphine oxide group. (b) All adducts are solid and crystallize readily in large habits. (c) The single crystal X-ray diffraction studies of **3**−**6** show that there is a common structural motif with two hydroperoxy groups hydrogen-bound to the oxygen of one P═O group. (d) All adducts are safe and robust toward high temperatures and mechanical stress inflicted by hammering and grinding, with shelf lives of months in a refrigerator. (e) The one-step synthesis of **3**−**6** is straightforward. (f) The high solubility of all adducts in organic solvents allows for natural abundance ^{17}O NMR spectroscopy. (g) The adducts can also be characterized by Raman and IR spectroscopy, both of which corroborate the hydrogen bonding of intact hydroperoxy groups. (h) ^{1}H DOSY spectroscopy revealed that the adducts **3**−**6** do not dissociate in solvents but diffuse through solutions as 1:1 assemblies. (i) Competition experiments using various phosphine oxides allowed the estimation of the relative strengths of the hydrogen bonds between the di(hydroperoxy)-cycloalkanes and the phosphine oxides with different electronic and steric properties. (j) Variable temperature ^{31}P NMR spectroscopy led to quantitative results on the migration of the di(hydroperoxy)cycloalkanes from one phosphine oxide carrier to the next, and the Gibbs energy of activation $\Delta G^{\ddagger}$, as well as the enthalpy and entropy of activation, $\Delta H^{\ddagger}$ and $\Delta S^{\ddagger}$, could be determined.

In the future, the toolbox of phosphine oxides for all adducts can be further expanded by including the oxides of tripodal phosphines[37] and tetraphosphines[36,91] as carriers to increase their specific peroxide contents.

In conclusion, the presented work greatly expands the general understanding, fundamental chemistry and characterization, as well as solution dynamics of a new important class of peroxides that are stabilized by novel P═O(···HOO)$_2$ hydrogen bonding motifs. They possess many of the most desirable attributes for oxidizing agents and are primed to have a significant positive impact on diverse problems in synthetic chemistry.

4. EXPERIMENTAL SECTION

4.a. General Considerations. All reactions were carried out using standard Schlenk techniques and a purified N_2 atmosphere, if not stated otherwise. Reagents purchased from Sigma-Aldrich or VWR were used without further purification. Aqueous H_2O_2 solution (35% w/w) was obtained from Acros Organics and used as received. Solvents were dried by boiling over sodium, then they were distilled and stored under purified nitrogen. Acetone, dichloromethane (Aldrich, ACS reagent grade), and ethanol (200 proof) were dried over 3 Å molecular sieves (EMD Chemical Inc.) prior to use. The latter were also used for drying **1** and **2**. The phosphine oxides were obtained according to literature procedures.[15,61] 1,1-Di-(hydroperoxy)cyclohexane and 1,1-di(hydroperoxy)cycloheptane were synthesized from cyclohexanone and cycloheptanone according to a literature procedure.[62]

4.b. Solubility Measurements of 3−6. The adduct (5−12 mg) was placed into a tared 20 mL vial. The desired solvent was added in drop-sized portions while the vial was shaken vigorously at 20 °C. Once all solid was dissolved, the overall weight gain was recorded, and the solvent volume was calculated.

4.c. NMR Spectroscopy. The ^{1}H, ^{13}C, and ^{31}P NMR spectra at ambient and variable temperatures were recorded at 499.70, 125.66, and 202.28 MHz on a 500 MHz Varian spectrometer. The ^{13}C and ^{31}P NMR spectra were recorded with ^{1}H decoupling if not stated otherwise. Neat Ph_2PCl ($\delta(^{31}P)$ = +81.92 ppm) in a capillary centered in the 5 mm NMR tubes was used for referencing the ^{31}P chemical shifts of dissolved compounds. For referencing the ^{1}H and ^{13}C chemical shifts, the residual proton and the carbon signals of the solvents were used (C_6D_6: $\delta(^{1}H)$ = 7.16 ppm, $\delta(^{13}C)$ = 128.00 ppm; $CDCl_3$: $\delta(^{1}H)$ = 7.26 ppm, $\delta(^{13}C)$ = 77.00 ppm). The signal assignments were based on comparisons with analogous phosphine oxides and 2D NMR spectra.[15,50,54−57]

^{17}O NMR Spectroscopy. The natural abundance ^{17}O NMR spectra were recorded using 0.3 to 0.5 molar benzene (C_6H_6) solutions of the compounds at 70 °C. A Varian 500 NMR spectrometer equipped with a 5 mm broad band probe operating at 67.79 MHz was employed. The following measurement parameters have been optimized to yield spectra of good quality with 0.8×10^6 to 1×10^6 scans: spectral window (73.5 kHz), number of data points (2206), measurement pulse length (20 μs), pulse angle (90°), relaxation delay (1 ms), and acquisition time (30 ms). The chemical shifts were referenced externally using pure D_2O ($\delta(^{17}O)$ = 0 ppm).

^{1}H DOSY. The ^{1}H DOSY NMR measurements were performed using a Varian 500 NMR spectrometer equipped with a 5 mm broad band probe operating at 499.84 MHz. Then, 0.015 molar solutions of the compounds in C_6D_6 were investigated at 25 °C. Hereby, 15 gradient increments were measured after optimizing the following parameters: pulse sequence (Dbppste), diffusion gradient length (1.75 ms), diffusion delay (50 ms), spectral window (8 kHz), complex points (16384), measurement pulse length (15 μs), pulse angle (90°), relaxation delay (1 s), acquisition time (2.045 s), number of scans (64), and number of steady state pulses (8). The measurements were performed using tetramethylsilane (TMS) as an internal size reference.[60] The diffusion (D) of the sample molecule was determined as the averaged values of D of all aromatic hydrogen atoms in the molecule, determined by integration. The ratio of the reference and sample diffusion ($\Delta r = D^{TMS}/D$) was multiplied with the van der Waals radius of TMS (7.34 Å) to give the hydrodynamic radius of the sample molecule.

4.d. IR Spectroscopy. The IR spectra of the neat powders of all adducts and compounds were recorded with a Shimadzu IRAffinity-1 FTIR spectrometer equipped with a Pike Technologies MIRacle ATR plate.

https://dx.doi.org/10.1021/acs.inorgchem.0c02087
Inorg. Chem. 2020, 59, 13719−13732

4.e. Raman Spectroscopy. The Raman spectra were acquired using a Jobin-Yvon Horiba Labram HR instrument coupled to an Olympus BX41 microscope with 514.51 nm laser excitation from an Ar-ion laser. A 600 lines/mm grating and an acquisition time of 2 s were applied. 60 scans gave spectra of good quality.

4.f. X-ray Diffraction. See the Supporting Information.

4.g. Synthesis and Characterization. *Synthesis of p-Tol$_3$PO (**1**).* *p*-Tol$_3$PO was synthesized according to a modified literature procedure.[92] *p*-Tol$_3$P (450 mg, 1.48 mmol) is dissolved in dichloromethane (14 mL), and aqueous H_2O_2 (6 mL, 35%, 70 mmol) is added while vigorously stirring. After 30 min, the phases are separated, and dry molecular sieves (550 mg) are added to the organic phase. After standing over the molecular sieves for 18 h, the solution is filtered, and the solvent is allowed to slowly evaporate. A colorless powder (467 mg, 1.46 mmol, 99% yield) is collected. Melting range: 142−146 °C.

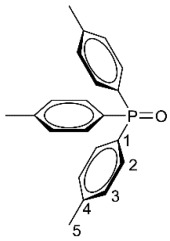

NMR (δ, $CDCl_3$), $^{31}P\{^1H\}$: 29.28 (s). ^1H: 7.52 (dd, $^3J(^{31}P-^1H)$ = 11.8 Hz, $^3J(^1H-^1H)$ = 8.1 Hz, 6H, H2), 7.21 (dd, $^3J(^1H-^1H)$ = 8.1 Hz, $^4J(^{31}P-^1H)$ = 2.4 Hz, 6H, H3), 2.34 (s, 9H, H5). ^{13}C: 142.18 (d, $^4J(^{31}P-^{13}C)$ = 2.8 Hz, C4), 132.04 (d, $^2J(^{31}P-^{13}C)$ = 10.2 Hz, C2), 129.13 (d, $^3J(^{31}P-^{13}C)$ = 12.5 Hz, C3), 128.58 (d, $^1J(^{31}P-^{13}C)$ = 80.8 Hz, C1), 21.56 ppm (d, $^5J(^{31}P-^{13}C)$ = 1.3 Hz, C5). IR: ν(P═O) = 1185 cm^{-1}.

*Synthesis of o-Tol$_3$PO (**2**).* The synthesis of **2** was performed according to a modified literature procedure.[92] (*o*-Tol$_3$PO·H_2O_2)$_2$ (6.99 g, 9.86 mmol) is dissolved in dichloromethane (100 mL), and dry molecular sieves (7 g) are added to the organic phase. After standing over molecular sieves for 18 h, the solution is filtered, and the solvent is allowed to slowly evaporate. A colorless powder (5.98 g, 18.7 mmol, 95% yield) is collected. Melting range: 134−137 °C. The crystal structure of **2** has been reported previously.[64] The NMR values are in correspondence with those given in the literature,[92] but no assignments have been provided.

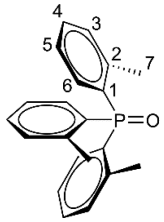

NMR (δ, $CDCl_3$), $^{31}P\{^1H\}$: 37.51 (s). ^1H: 7.44 (t, $^3J(^1H-^1H)$ = 7.4 Hz, 3H, H4), 7.32 (dd, $^3J(^1H-^1H)$ = 7.6 Hz, $^4J(^{31}P-^1H)$ = 4.1 Hz, 3H, H3), 7.20−7.16 (m, 3H, H5), 7.10 (ddd, $^3J(^{31}P-^1H)$ = 13.8 Hz, $^3J(^1H-^1H)$ = 7.7 Hz, $^4J(^1H-^1H)$ = 1.3 Hz, 3H, H6), 2.50 (s, 9H, H7). ^{13}C: 143.69 (d, $^2J(^{31}P-^{13}C)$ = 7.8 Hz, C2), 133.07 (d, $^2J(^{31}P-^{13}C)$ = 12.8 Hz, C6), 132.17 (d, $^3J(^{31}P-^{13}C)$ = 10.4 Hz, C3), 132.05 (d, $^4J(^{31}P-^{13}C)$ = 2.6 Hz, C4), 128.77 (d, $^1J(^{31}P-^{13}C)$ = 81.5 Hz, C1), 125.65 (d, $^3J(^{31}P-^{13}C)$ = 12.8 Hz, C5), 22.15 ppm (d, $^3J(^{31}P-^{13}C)$ = 4.1 Hz, C7). IR: ν(P═O) = 1158 cm^{-1}.

*Synthesis of p-Tol$_3$PO·(HOO)$_2$C(CH$_2$)$_5$ (**3**).* *p*-Tol$_3$PO (450 mg, 1.40 mmol) is dissolved in dichloromethane (10 mL), and 1,1-di(hydroperoxy)cyclohexane (250 mg, 1.69 mmol) is added under stirring. Hexanes (10 mL) is added to the mixture, and the solvent is allowed to evaporate slowly. Large colorless crystals (487 mg, 1.04 mmol, 74% yield) are obtained. Melting range: 114−115 °C.

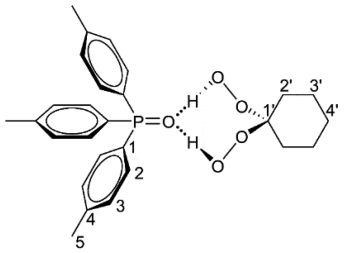

NMR (δ, $CDCl_3$), $^{31}P\{^1H\}$: 34.76 (s). ^1H: 9.31−8.35 (br s, O*H*), 7.54 (dd, $^3J(^{31}P-^1H)$ = 12.1 Hz, $^3J(^1H-^1H)$ = 7.8 Hz, 6H, H2), 7.28 (d, $^3J(^1H-^1H)$ = 7.6 Hz, 6H, H3), 2.41 (s, 9H, H5), 1.85 (t, $^3J(^1H-^1H)$ = 6.1 Hz, 4H, H2′), 1.60 (quint., $^3J(^1H-^1H)$ = 6.1 Hz, 4H, H3′), 1.52−1.43 (m, 2H, H4′). ^{13}C: 143.00 (d, $^4J(^{31}P-^{13}C)$ = 2.6 Hz, C4), 132.26 (d, $^2J(^{31}P-^{13}C)$ = 10.7 Hz, C2), 129.52 (d, $^3J(^{31}P-^{13}C)$ = 12.8 Hz, C3), 128.15 (d, $^1J(^{31}P-^{13}C)$ = 108.3 Hz, C1), 109.50 (s, C1′), 29.94 (s, C2′), 25.82 (s, C4′), 22.75 (s, C3′), 21.74 ppm (d, $^5J(^{31}P-^{13}C)$ = 1.3 Hz, C5). IR: ν(O−H) = 3254 cm^{-1}, ν(P═O) = 1150 cm^{-1}.

*Synthesis of o-Tol$_3$PO·(HOO)$_2$C(CH$_2$)$_5$ (**4**).* *o*-Tol$_3$PO (450 mg, 1.40 mmol) is dissolved in dichloromethane (10 mL), and 1,1-di(hydroperoxy)cyclohexane (250 mg, 1.69 mmol) is added while stirring. Hexanes (10 mL) is added to the mixture, and the solvent is allowed to evaporate slowly. Colorless crystals (587 mg, 1.25 mmol, 89% yield) are collected. Melting range: 138−140 °C.

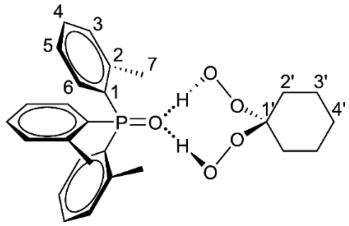

NMR (δ, $CDCl_3$), $^{31}P\{^1H\}$: 42.47 (s). ^1H: 9.74−8.20 (br s, O*H*), 7.46 (t, $^3J(^1H-^1H)$ = 7.5 Hz, 3H, H4), 7.34 (dd, $^3J(^1H-^1H)$ = 7.4 Hz, $^4J(^{31}P-^1H)$ = 4.4 Hz, 3H, H3), 7.17 (t, $^3J(^1H-^1H)$ = 7.2 Hz, 3H, H5), 7.06 (dd, $^3J(^{31}P-^1H)$ = 14.5 Hz, $^3J(^1H-^1H)$ = 7.7 Hz, 3H, H6), 2.47 (s, 9H, H7), 1.79 (t, $^3J(^1H-^1H)$ = 6.2 Hz, 4H, H2′), 1.62−1.52 (m, 4H, H3′), 1.44−1.39 (m, 2H, H4′). ^{13}C: 143.77 (d, $^2J(^{31}P-^{13}C)$ = 7.7 Hz, C2), 133.17 (d, $^2J(^{31}P-^{13}C)$ = 13.5 Hz, C6), 132.60 (d, not fully resolved, C4), 132.45 (d, $^3J(^{31}P-^{13}C)$ = 10.5 Hz, C3), 129.07 (d, $^1J(^{31}P-^{13}C)$ = 101.1 Hz, C1), 125.85 (d, $^3J(^{31}P-^{13}C)$ = 13.2 Hz, C5), 109.40 (s, C1′), 29.88 (s, C2′), 25.78 (s, C4′), 22.73 (s, C3′), 22.14 ppm (d, $^3J(^{31}P-^{13}C)$ = 4.3 Hz, C7). IR: ν(O−H) = 3240 cm^{-1}, ν(P═O) = 1146 cm^{-1}.

*Synthesis of p-Tol$_3$PO·(HOO)$_2$C(CH$_2$)$_6$ (**5**).* *p*-Tol$_3$PO (450 mg, 1.40 mmol) is dissolved in dichloromethane (10 mL), and 1,1-di(hydroperoxy)cycloheptane (226 mg, 1.4 mmol) is added under stirring. Hexanes (10 mL) is added to the reaction mixture, and the solvent is allowed to evaporate slowly. Colorless crystals (523 mg, 1.08 mmol, 78% yield) have been collected. Melting range: 120−122 °C. After melting, oxygen was released at 126 °C.

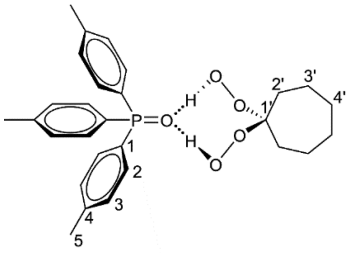

NMR (δ, $CDCl_3$), $^{31}P\{^1H\}$: 32.51 (s). ^1H: 7.49 (dd, $^3J(^{31}P-^1H)$ = 12.0 Hz, $^3J(^1H-^1H)$ = 7.9 Hz, 6H, H2), 7.22 (d, $^3J(^1H-^1H)$ = 7.7 Hz, 6H, H3), 6.35−5.33 (br s, O*H*), 2.36 (s, 9H, H5), 1.94−1.90 (m,

https://dx.doi.org/10.1021/acs.inorgchem.0c02087
Inorg. Chem. 2020, 59, 13719−13732

4H, H2′), 1.59−1.50 (m, 8H, H3′, H4′). ^{13}C: 142.78 (d, $^{4}J(^{31}P-^{13}C)$ = 2.3 Hz, C4), 132.27 (d, $^{2}J(^{31}P-^{13}C)$ = 10.5 Hz, C2), 129.44 (d, $^{3}J(^{31}P-^{13}C)$ = 12.7 Hz, C3), 128.76 (d, $^{1}J(^{31}P-^{13}C)$ = 106.5 Hz, C1), 114.71 (s, C1′), 32.56 (s, C2′), 30.31 (s, C4′), 23.04 (s, C3′), 21.75 ppm (d, $^{5}J(^{31}P-^{13}C)$ = 1.3 Hz, C5). IR: ν(O−H) = 3275 cm^{-1}, ν(P═O) = 1150 cm^{-1}.

*Synthesis of o-Tol$_3$PO·(HOO)$_2$C(CH$_2$)$_6$ (**6**).* *o*-Tol$_3$PO (450 mg, 1.40 mmol) is dissolved in dichloromethane (10 mL), and 1,1-di(hydroperoxy)cycloheptane (226 mg, 1.4 mmol) is added while stirring. Hexanes (10 mL) is added to the reaction mixture, and the solvent is allowed to slowly evaporate. Colorless crystals (504 mg, 1.04 mmol, 75% yield) are collected. Melting range: 119−130 °C.

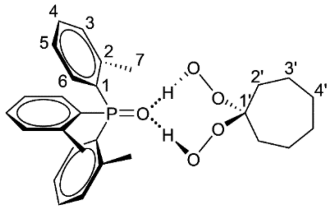

NMR (δ, $CDCl_3$), $^{31}P\{^{1}H\}$: 39.95 (s). ^{1}H: 7.44 (t, $^{3}J(^{1}H-^{1}H)$ = 7.5 Hz, 3H, H4), 7.32 (dd, $^{3}J(^{1}H-^{1}H)$ = 7.6 Hz, $^{4}J(^{31}P-^{1}H)$ = 4.2 Hz, 3H, H3), 7.15 (t, $^{3}J(^{1}H-^{1}H)$ = 7.2 Hz, 3H, H5), 7.07 (dd, $^{3}J(^{31}P-^{1}H)$ = 14.3 Hz, $^{3}J(^{1}H-^{1}H)$ = 7.5 Hz, 3H, H6), 2.48 (s, 9H, H7), 1.92−1.90 (m, 4H, H2′), 1.59−1.50 (m, 8H, H3′, H4′). ^{13}C: 143.72 (d, $^{2}J(^{31}P-^{13}C)$ = 7.7 Hz, C2), 133.10 (d, $^{2}J(^{31}P-^{13}C)$ = 13.1 Hz, C6), 132.29 (d, $^{3}J(^{31}P-^{13}C)$ = 10.5 Hz, C3), 132.28 (d, $^{4}J(^{31}P-^{13}C)$ = 2.6 Hz, C4), 129.91 (d, $^{1}J(^{31}P-^{13}C)$ = 102.2 Hz, C1), 125.72 (d, $^{3}J(^{31}P-^{13}C)$ = 13.0 Hz, C5), 114.60 (s, C1′), 32.44 (s, C2′), 30.33 (s, C4′), 22.99 (s, C3′), 22.11 ppm (d, $^{3}J(^{31}P-^{13}C)$ = 4.1 Hz, C7). IR: ν(O−H) = 3246 cm^{-1}, ν(P═O) = 1152 cm^{-1}.

■ ASSOCIATED CONTENT

Supporting Information

The Supporting Information is available free of charge at https://pubs.acs.org/doi/10.1021/acs.inorgchem.0c02087.

Detailed description of materials and methods used for X-ray crystallography; crystallographic information for **1** and **3**−**6** with selected data in tables; dynamic NMR spectra and corresponding gNMR simulations, Eyring plots, and a table summarizing variable temperature ^{31}P NMR chemical shift and line width data (PDF)

Accession Codes

CCDC 1937469 (**1**), 1960850 (**3**), 1960851 (**4**), 1960852 (**5**), 1960853 (**6**) contain the crystallographic data for this paper. These data can be obtained free of charge via www.ccdc.cam.ac.uk/data_request/cif, or by emailing data_request@ccdc.cam.ac.uk, or by contacting TheCambridge Crystallographic Data Centre, 12 Union Road, Cambridge CB2 1EZ, UK; fax: + 44 1223 336033.

■ AUTHOR INFORMATION

Corresponding Author

Janet Blümel − *Department of Chemistry, Texas A&M University, College Station, Texas 77842-3012, United States*; Email: bluemel@tamu.edu

Authors

Fabian F. Arp − *Department of Chemistry, Texas A&M University, College Station, Texas 77842-3012, United States*

Nattamai Bhuvanesh − *Department of Chemistry, Texas A&M University, College Station, Texas 77842-3012, United States*

Complete contact information is available at: https://pubs.acs.org/10.1021/acs.inorgchem.0c02087

Notes

The authors declare no competing financial interest.

■ ACKNOWLEDGMENTS

This work was supported by the National Science Foundation (CHE-1300208 and CHE-1900100).

■ REFERENCES

(1) Duprey, D.; Cavani, F. *Handbook of Advanced Methods and Processes in Oxidation Catalysis*; Imperial College Press, 2014.

(2) Cavani, F.; Teles, J. H. Sustainability in Catalytic Oxidation: An Alternative Approach or a Structural Evolution? *ChemSusChem* **2009**, *2*, 508−534.

(3) Comyns, A. E. Peroxides and Peroxide Compounds. *Van Nostrand's Encyclopedia of Chemistry*; John Wiley & Sons, Inc., 2005.

(4) Todorović, N. M.; Stefanovic, M.; Tinant, B.; Declercq, J.-P.; Makler, M. T.; Šolaja, B. A. Steroidal geminal dihydroperoxides and 1,2,4,5-tetraoxanes: Structure determination and their antimalarial activity. *Steroids* **1996**, *61*, 688−696.

(5) Bettenhausen, C. A. Treating wastewater with peracetic acid. *Chem. Eng. News* **2020**, *98*, 16−18.

(6) Krylov, I. B.; Budnikov, A. S.; Lastovko, A. V.; Ibatov, Y. A.; Nikishin, G. I.; Terent'ev, A. O. Addition of N-hydroxyphthalimide and atmospheric oxygen to styrenes using tert-butyl hydroperoxide as a radical initiator. *Russ. Chem. Bull.* **2019**, *68*, 1454−1457.

(7) Legacy, C. J.; Wang, A.; O'Day, B. J.; Emmert, M. H. Iron-Catalyzed C_α-H Oxidation of Tertiary, Aliphatic Amines to Amides under Mild Conditions. *Angew. Chem., Int. Ed.* **2015**, *54*, 14907−14910.

(8) Legacy, C. J.; Emmert, M. H. C_α-H Oxidations of Amines to Amides: Expanding Mechanistic Understanding and Amine Scope through Catalyst Development. *Synlett* **2016**, *27*, 1893−1897.

(9) Osberger, T. J.; Rogness, D. C.; Kohrt, J. T.; Stepan, A. F.; White, M. C. Oxidative Diversification of Amino Acids and Peptides by Small-Molecule Iron Catalysis. *Nature* **2016**, *537*, 214−219.

(10) Howell, J. M.; Feng, K.; Clark, J. R.; Trzepkowski, L. J.; White, M. C. Remote Oxidation of Aliphatic C-H Bonds in Nitrogen-Containing Molecules. *J. Am. Chem. Soc.* **2015**, *137*, 14590−14593.

(11) Zhou, M. D.; Liu, M.; Huang, J.; Zhang, J.; Wang, J.; Li, X.; Kühn, F. E.; Zang, S. L. Olefin Epoxidation with Hydrogen Peroxide using Octamolybdate-Based Self-Separating Catalysts. *Green Chem.* **2015**, *17*, 1186−1193.

(12) Markovits, I. I. E.; Eger, W. A.; Yue, S.; Cokoja, M.; Münchmeyer, C. J.; Zhang, B.; Zhou, M.-D.; Genest, A.; Mink, J.; Zang, S.-L.; Rösch, N.; Kühn, F. E. Activation of Hydrogen Peroxide by Ionic Liquids: Mechanistic Studies and Application in the Epoxidation of Olefins. *Chem. - Eur. J.* **2013**, *19*, 5972−5979.

(13) Wojaczynska, E.; Wojaczynski, J. Enantioselective Synthesis of Sulfoxides. *Chem. Rev.* **2010**, *110*, 4303−4356.

(14) Bulman Page, P.; Buckley, B.; Elliott, C.; Chan, Y.; Dreyfus, N.; Marken, F. Chemoselective Oxidation of Sulfides to Sulfoxides with Urea-Hydrogen Peroxide Complex Catalysed by Diselenide. *Synlett* **2015**, *27*, 80−82.

(15) Hilliard, C. R.; Bhuvanesh, N.; Gladysz, J. A.; Blümel, J. Synthesis, Purification, and Characterization of Phosphine Oxides and Their Hydrogen Peroxide Adducts. *Dalton Trans.* **2012**, *41*, 1742−1754.

(16) Chrzanowski, J.; Krasowska, D.; Drabowicz, J. Synthesis of Optically Active Tertiary Phosphine Oxides: A Historical Overview and the Latest Advances. *Heteroat. Chem.* **2018**, *29*, No. e21476.

(17) Uyanik, M.; Ishihara, K. Baeyer-Villiger Oxidation Using Hydrogen Peroxide. *ACS Catal.* **2013**, *3*, 513−520.

(18) Zhou, L.; Liu, X.; Ji, J.; Zhang, Y.; Hu, X.; Lin, L.; Feng, X. Enantioselective Baeyer-Villiger Oxidation: Desymmetrization of Meso Cyclic Ketones and Kinetic Resolution of Racemic 2-Arylcyclohexanones. *J. Am. Chem. Soc.* **2012**, *134*, 17023−17026.

(19) Ji, L.; Wang, Y.-N.; Qian, C.; Chen, X.-Z. Nitrile-Promoted Alkene Epoxidation with Urea-Hydrogen Peroxide (UHP). *Synth. Commun.* **2013**, *43*, 2256−2264.
(20) Kaur, D.; Chhabra, B. R. Silica Supported Urea-Hydrogen Peroxide as a Source of Oxygen. *J. Chem. Biol., Phys. Sci. A* **2013**, *3*, 980−987.
(21) Koukabi, N. Sodium Percarbonate: A Versatile Oxidizing Reagent. *Synlett* **2010**, *2010*, 2969−2970.
(22) Churakov, A. V.; Prikhodchenko, P. V.; Howard, J. A. K. The preparation and crystal structures of novel perhydrates $Ph_4X^+Hal^-\cdot nH_2O_2$: anionic hydrogen-bonded chains containing hydrogen peroxide. *CrystEngComm* **2005**, *7*, 664−669.
(23) Churakov, A. V.; Grishanov, D. A.; Medvedev, A. G.; Mikhaylov, A. A.; Vener, M. V.; Navasardyan, M. A.; Tripol'skaya, T. A.; Lev, O.; Prikhodchenko, P. V. Stabilization of hydrogen peroxide by hydrogen bonding in the crystal structure of 2-aminobenzimidazole perhydrate. *CrystEngComm* **2020**, *22*, 2866−2872.
(24) McKillop, A.; Sanderson, W. R. Sodium perborate and sodium percarbonate: further applications in organic synthesis. *J. Chem. Soc., Perkin Trans. 1* **2000**, 471−476.
(25) Gómez, M. V.; Caballero, R.; Vázquez, E.; Moreno, A.; de la Hoz, A.; Díaz-Ortiz, Á. Green and chemoselective oxidation of sulfides with sodium perborate and sodium percarbonate: nucleophilic and electrophilic character of the oxidation system. *Green Chem.* **2007**, *9*, 331−336.
(26) Elkhayat, Z.; Safir, I.; Gandara, Z.; Retailleau, P.; Arseniyadis, S. Efficient Construction of Highly Substituted and Stereodefined cis-Fused Lactones. *Eur. J. Org. Chem.* **2010**, *2010*, 4851−4860.
(27) Ganguly, N. C.; Chandra, S.; Barik, S. K. Sodium Perborate Tetrahydrate−Mediated Transformations of 2′-Hydroxychalcones to Flavanones, Flavones, and 3′, 5′-Diiodoflavone Under Mild, Environmentally Friendly Conditions. *Synth. Commun.* **2013**, *43*, 1351−1361.
(28) Arzumanyan, A. V.; Novikov, R. A.; Terent'ev, A. O.; Platonov, M. M.; Lakhtin, V. G.; Arkhipov, D. E.; Korlyukov, A. A.; Chernyshev, V. V.; Fitch, A. N.; Zdvizhkov, A. T.; Krylov, I. B.; Tomilov, Y. V.; Nikishin, G. I. Nature Chooses Rings: Synthesis of Silicon-Containing Macrocyclic Peroxides. *Organometallics* **2014**, *33*, 2230−2246.
(29) Kharel, S.; Jia, T.; Bhuvanesh, N.; Reibenspies, J. H.; Blümel, J.; Gladysz, J. A. A Non-templated Route to Macrocyclic Dibridgehead Diphosphorus Compounds: Crystallographic Characterization of a "Crossed-Chain" Variant of *in/out* Stereoisomers. *Chem. - Asian J.* **2018**, *13*, 2632−2640.
(30) Fletcher, M. D. Phospho-transfer Processes Leading to [P-C] Bond Formation. *Organophosphorus Reagents*; Oxford University Press, 2004; pp 171−214.
(31) Adams, H.; Collins, R. C.; Jones, S.; Warner, C. J. A. Enantioselective Preparation of P-Chiral Phosphine Oxides. *Org. Lett.* **2011**, *13*, 6576−6579.
(32) Swamy, K. C. K.; Kumar, N. N. B.; Balaraman, E.; Kumar, K. V. P. P. Mitsunobu and Related Reactions: Advances and Applications. *Chem. Rev.* **2009**, *109*, 2551−2651.
(33) Beddoe, R. H.; Andrews, K. G.; Magne, V.; Cuthbertson, J. D.; Saska, J.; Shannon-Little, A. L.; Shanahan, S. E.; Sneddon, H. F.; Denton, R. M. Redox-Neutral Organocatalytic Misunobu Reactions. *Science* **2019**, *365*, 910−914.
(34) Guenther, J.; Reibenspies, J.; Blümel, J. Synthesis and Characterization of Tridentate Phosphine Ligands Incorporating Long Methylene Chains and Ethoxysilane Groups for Immobilizing Molecular Rhodium Catalysts. *Mol. Catal.* **2019**, *479*, 110629.
(35) Pope, J. C.; Posset, T.; Bhuvanesh, N.; Blümel, J. The Palladium Component of an Immobilized Sonogashira Catalyst System: New Insights by Multinuclear HRMAS NMR Spectroscopy. *Organometallics* **2014**, *33*, 6750−6753.
(36) Baker, J. H.; Bhuvanesh, N.; Blümel, J. Tetraphosphines with Tetra(biphenyl)silane and -Stannane Cores as Rigid Scaffold Linkers for Immobilized Catalysts. *J. Organomet. Chem.* **2017**, *847*, 193−203.
(37) Cluff, K. J.; Bhuvanesh, N.; Blümel, J. Monometallic Ni(0) and Heterobimetallic Ni(0)/Au(I) Complexes of Tripodal Phosphine Ligands: Characterization in Solution and in the Solid State and Catalysis. *Chem. - Eur. J.* **2015**, *21*, 10138−10148.
(38) Zheng, A.; Liu, S.-B.; Deng, F. ^{31}P NMR Chemical Shifts of Phosphorus Probes as Reliable and Practical Acidity Scales for Solid and Liquid Catalysts. *Chem. Rev.* **2017**, *117*, 12475−12531.
(39) Machida, S.; Sohmiya, M.; Ide, Y.; Sugahara, Y. Solid-State ^{31}P Nuclear Magnetic Resonance Study of Interlayer Hydroxide Surfaces of Kaolinite Probed with an Interlayer Triethylphosphine Oxide Monolayer. *Langmuir* **2018**, *34*, 12694−12701.
(40) Wilmsmeyer, A. R.; Gordon, W. O.; Davis, E. D.; Mantooth, B. A.; Lalain, T. A.; Morris, J. R. Multifunctional Ultra-High Vacuum Apparatus for Studies of the Interactions of Chemical Warfare Agents on Complex Surfaces. *Rev. Sci. Instrum.* **2014**, *85*, 014101.
(41) Hubbard, P. J.; Benzie, J. W.; Bakhmutov, V. I.; Blümel, J. Disentangling Different Modes of Mobility of Triphenylphosphine Oxide Adsorbed on Alumina. *J. Chem. Phys.* **2020**, *152*, 054718.
(42) Kharel, S.; Cluff, K. J.; Bhuvanesh, N.; Gladysz, J. A.; Blümel, J. Structures and Dynamics of Secondary and Tertiary Alkylphosphine Oxides Adsorbed on Silica. *Chem. - Asian J.* **2019**, *14*, 2704−2711.
(43) Hilliard, C. R.; Kharel, S.; Cluff, K. J.; Bhuvanesh, N.; Gladysz, J. A.; Blümel, J. Structures and Unexpected Dynamic Properties of Phosphine Oxides Adsorbed on Silica Surfaces. *Chem. - Eur. J.* **2014**, *20*, 17292−17295.
(44) Stross, A. E.; Iadevaia, G.; Hunter, C. A. Cooperative Duplex Formation by Synthetic H-Bonding Oligomers. *Chem. Sci.* **2016**, *7*, 94−101.
(45) Nunez-Villanueva, D.; Hunter, C. A. Homochiral Oligomers with Highly Flexible Backbones from Stable H-Bonded Duplexes. *Chem. Sci.* **2017**, *8*, 206−213.
(46) Bewick, N. A.; Arendt, A.; Li, Y.; Szafert, S.; Lis, T.; Wheeler, K. A.; Young, J.; Dembinski, R. Synthesis and Solid-State Structure of (4-Hydroxy-3,5-diiodophenyl)phosphine Oxides. Dimeric Motifs with the Assistance of O-H· · ·O = P Hydrogen Bonds. *Curr. Org. Chem.* **2015**, *19*, 469−474.
(47) Pike, S. J.; Hunter, C. A. Fluorescent and Colorimetric Molecular Recognition Probe for Hydrogen Bond Acceptors. *Org. Biomol. Chem.* **2017**, *15*, 9603−9610.
(48) Burke, N. J.; Burrows, A. D.; Mahon, M. F.; Warren, J. E. Hydrogen Bond Network Structures Based on Sulfonated Phosphine Ligands: The Effects of Complex Geometry, Cation Substituents and Phosphine Oxidation on Guanidinium Sulfonate Sheet Formation. *Inorg. Chim. Acta* **2006**, *359*, 3497−3506.
(49) Joshi, R.; Pasilis, S. P. The Effect of Tributylphosphate and Tributylphosphine Oxide on Hydrogen Bonding Interactions between Water and the 1-Ethyl-3-methylimidazolium Cation in 1-Ethyl-3-Methylimidazolium bis(trifluoromethylsulfonyl)imide. *J. Mol. Liq.* **2015**, *209*, 381−386.
(50) Arp, F. F.; Bhuvanesh, N.; Blümel, J. Hydrogen Peroxide Adducts of Triarylphosphine Oxides. *Dalton Trans.* **2019**, *48*, 14312−14325.
(51) Kharel, S.; Bhuvanesh, N.; Gladysz, J. A.; Blümel, J. New Hydrogen Bonding Motifs of Phosphine Oxides with a Silanediol, a Phenol, and Chloroform. *Inorg. Chim. Acta* **2019**, *490*, 215−219.
(52) Tupikina, E. Y.; Bodensteiner, M.; Tolstoy, P. M.; Denisov, G. S.; Shenderovich, I. G. P═O Moiety as an Ambidextrous Hydrogen Bond Acceptor. *J. Phys. Chem. C* **2018**, *122*, 1711−1720.
(53) Begimova, G.; Tupikina, E. Y.; Yu, V. K.; Denisov, G. S.; Bodensteiner, M.; Shenderovich, I. G. Effect of Hydrogen Bonding to Water on the ^{31}P Chemical Shift Tensor of Phenyl- and Trialkylphosphine Oxides and α-Amino Phosphonates. *J. Phys. Chem. C* **2016**, *120*, 8717−8729.
(54) Arp, F. F.; Ahn, S. H.; Bhuvanesh, N.; Blümel, J. Selective Synthesis and Stabilization of Peroxides via Phosphine Oxides. *New J. Chem.* **2019**, *43*, 17174−17181.
(55) Ahn, S. H.; Cluff, K. J.; Bhuvanesh, N.; Blümel, J. Hydrogen Peroxide and Di(hydroperoxy)propane Adducts of Phosphine Oxides as Stoichiometric and Soluble Oxidizing Agents. *Angew. Chem., Int. Ed.* **2015**, *54*, 13341−13345.

https://dx.doi.org/10.1021/acs.inorgchem.0c02087
Inorg. Chem. 2020, 59, 13719−13732

(56) Ahn, S. H.; Bhuvanesh, N.; Blümel, J. Di(hydroperoxy)alkane Adducts of Phosphine Oxides: Safe, Solid, Stoichiometric, and Soluble Oxidizing Agents. *Chem. - Eur. J.* **2017**, *23*, 16998−17009.
(57) Ahn, S. H.; Lindhardt, D.; Bhuvanesh, N.; Blümel, J. Di(hydroperoxy)cycloalkanes Stabilized via Hydrogen Bonding by Phosphine Oxides: Safe and Efficient Baeyer-Villiger Oxidants. *ACS Sustainable Chem. Eng.* **2018**, *6*, 6829−6840.
(58) Cook, J. L.; Hunter, C. A.; Low, C. M. R.; Perez-Velasco, A.; Vinter, J. G. Solvent Effects on Hydrogen Bonding. *Angew. Chem., Int. Ed.* **2007**, *46*, 3706−3709.
(59) Kagan, G.; Li, W.; Hopson, R.; Williard, P. G. Internally Referenced Diffusion Coefficient-Formula Weight (D-FW) Analysis of ^{31}P Diffusion-Ordered NMR Spectroscopy (DOSY). *Org. Lett.* **2009**, *11*, 4818−4821.
(60) Cabrita, E. J.; Berger, S. DOSY studies of hydrogen bond association: tetramethylsilane as a reference compound for diffusion studies. *Magn. Reson. Chem.* **2001**, *39*, S142−S148.
(61) Burger, A.; Dawson, N. D. The Reaction of Dialkyl Chlorophosphates with Arylmagnesium Halides. *J. Org. Chem.* **1951**, *16*, 1250−1254.
(62) Terent'ev, A. O.; Platonov, M. M.; Ogibin, Y. N.; Nikishin, G. I. Convenient Synthesis of Geminal Bishydroperoxides by the Reaction of Ketones with Hydrogen Peroxide. *Synth. Commun.* **2007**, *37*, 1281−1287.
(63) Etter, M. C.; Baures, P. W. Triphenylphosphine Oxide as a Crystallization Aid. *J. Am. Chem. Soc.* **1988**, *110*, 639−640.
(64) Fronczek, F. R. CCDC 1021095. *CSD Communication*; **2014**, DOI: 10.5517/cc138jkg.
(65) Jeffrey, G. A. *An Introduction to Hydrogen Bonding*; Oxford University Press: Oxford, 1997.
(66) Baker, E. N.; Hubbard, R. E. Hydrogen Bonding in Globular Proteins. *Prog. Biophys. Mol. Biol.* **1984**, *44*, 97−179.
(67) De Silva, N.; Zahariev, F.; Hay, B. P.; Gordon, M. S.; Windus, T. L. *J. Phys. Chem. A* **2015**, *119*, 8765−8773.
(68) McFarlane, H. C. E.; McFarlane, W. *Oxygen in Multinuclear NMR*; Mason, J., Ed.; Plenum Press, New York, 1987.
(69) Barieux, J. J.; Schirmann, J. P. ^{17}O-enriched hydrogen peroxide and t-butyl hydroperoxide: Synthesis, characterization and some applications. *Tetrahedron Lett.* **1987**, *28*, 6443.
(70) Plesničar, B.; Cerkovnik, J.; Tekavec, T.; Koller, J. ^{17}O NMR Spectroscopic Characterization and the Mechanism of Formation of Alkyl Hydrotrioxides (ROOOH) and Hydrogen Trioxide (HOOOH) in the Low-Temperature Ozonation of Isopropyl Alcohol and Isopropyl Methyl Ether: Water-Assisted Decomposition. *Chem. - Eur. J.* **2000**, *6*, 809−819.
(71) Čásný, M.; Rehder, D.; Schmidt, H.; Vilter, H.; Conte, V. A ^{17}O NMR study of peroxide binding to the active centre of bromoperoxidase from Ascophyllum nodosum. *J. Inorg. Biochem.* **2000**, *80*, 157−160.
(72) Alam, T. M.; Celina, M.; Assink, R. A.; Clough, R. L.; Gillen, K. T.; Wheeler, D. R. Investigation of Oxidative Degradation in Polymers Using ^{17}O NMR Spectroscopy. *Macromolecules* **2000**, *33*, 1181−1190.
(73) Bryce, D. L.; Eichele, K.; Wasylishen, R. E. An ^{17}O NMR and Quantum Chemical Study of Monoclinic and Orthorhombic Polymorphs of Triphenylphosphine Oxide. *Inorg. Chem.* **2003**, *42*, 5085−5096.
(74) Wong, A.; Pike, K. J.; Jenkins, R.; Clarkson, G. J.; Anupõld, T.; Howes, A. P.; Crout, D. H. G.; Samoson, A.; Dupree, R.; Smith, M. E. Experimental and Theoretical ^{17}O NMR Study of the Influence of Hydrogen-Bonding on C = O and O-H Oxygens in Carboxylic Solids. *J. Phys. Chem. A* **2006**, *110*, 1824−1835.
(75) Dahn, H.; Van Toan, V.; Ung-Truong, M.-N. NMR of terminal oxygen. 9-^{17}O NMR of the P-O 'double bond': Phosphine oxides, phosphinates, phosphonates, acylphosphonates and related compounds. *Magn. Reson. Chem.* **1992**, *30*, 1089−1096.
(76) Sammons, R. D.; Frey, P. A.; Bruzik, K.; Tsai, M.-D. Effects of oxygen-17 and oxygen-18 on phosphorus-31 NMR: further investigation and applications. *J. Am. Chem. Soc.* **1983**, *105*, 5455−5461.
(77) Baumstark, A. L.; Vasquez, P. C.; Balakrishnan, P. ^{17}O-enriched α-azohydroperoxides: ^{17}O NMR spectroscopy, ^{17}O-labeling reagents. *Tetrahedron Lett.* **1985**, *26*, 2051−2054.
(78) Budzelaar, P. H. M. *gNMR 5.0.6.0; IvorySoft: Centennial*, CO, 2006.
(79) Ašperger, S. *Chemical Kinetics and Inorganic Reaction Mechanisms*; Kluwer Academic/Plenum Publishers, 2003.
(80) Zimmer, D. K.; Shoemaker, R.; Ruminski, R. R. Synthesis and characterization of a fluxional Re(I) carbonyl complex fac-[Re(CO)$_3$(dpop′)Cl] with the nominally tri-dentate ligand dipyrido(2,3-a:3′,2′-j)phenazine (dpop′). *Inorg. Chim. Acta* **2006**, *359*, 1478−1484.
(81) Sheu, S.-Y.; Yang, D.-Y.; Selzle, H. L.; Schlag, E. W. Energetics of hydrogen bonds in peptides. *Proc. Natl. Acad. Sci. U. S. A.* **2003**, *100*, 12683−12687.
(82) Guthrie, J. P. Intrinsic Barriers for Proton Transfer Reactions Involving Electronegative Atoms, and the Water Mediated Proton Switch: An Analysis in Terms of Marcus Theory. *J. Am. Chem. Soc.* **1996**, *118*, 12886−12890.
(83) Günzler, H.; Gremlich, H.-U. *IR Spektroskopie*, 4th ed.; Wiley-VCH, 2003.
(84) Tsuneda, T.; Miyake, J.; Miyatake, K. Mechanism of H_2O_2 Decomposition by Triphenylphosphine Oxide. *ACS Omega* **2018**, *3*, 259−265.
(85) Fletcher, W. H.; Rayside, J. S. High resolution vibrational Raman spectrum of oxygen. *J. Raman Spectrosc.* **1974**, *2*, 3−14.
(86) Hayyan, M.; Hashim, M. A.; AlNashef, I. M. Superoxide Ion: Generation and Chemical Implications. *Chem. Rev.* **2016**, *116*, 3029−3085.
(87) Taylor, R. C.; Cross, P. C. Raman Spectra of Hydrogen Peroxide in Condensed Phases. I. The Spectra of the Pure Liquid and Its Aqueous Solutions. *J. Chem. Phys.* **1956**, *24*, 41−44.
(88) Giguére, P. A.; Srinivasan, T. K. K. A Raman study of H_2O_2 and D_2O_2 vapor. *J. Raman Spectrosc.* **1974**, *2*, 125−132.
(89) Eysel, H. H.; Thym, S. RAMAN Spectra of Peroxides. *Z. Anorg. Allg. Chem.* **1975**, *411*, 97−102.
(90) Vacque, V.; Sombret, B.; Huvenne, J. P.; Legrand, P.; Suc, S. Characterisation of the O-O peroxide bond by vibrational spectroscopy. *Spectrochim. Acta, Part A* **1997**, *53*, 55−66.
(91) Yang, Y.; Beele, B.; Blümel, J. Easily Immobilized Di- and Tetraphosphine Linkers: Rigid Scaffolds that Prevent Interactions of Metal Complexes with Oxide Supports. *J. Am. Chem. Soc.* **2008**, *130*, 3771−3773.
(92) Denton, R. M.; An, J.; Adeniran, B.; Blake, A. J.; Lewis, W.; Poulton, A. M. Catalytic Phosphorus(V)-Mediated Nucleophilic Substitution Reactions: Development of a Catalytic Appel Reaction. *J. Org. Chem.* **2011**, *76*, 6749−6767.

https://dx.doi.org/10.1021/acs.inorgchem.0c02087
Inorg. Chem. 2020, 59, 13719−13732